JGR Solid Earth

RESEARCH ARTICLE
10.1029/2024JB030268

Crustal Structure of the Hikurangi Subduction Zone Revealed by Four Decades of Onshore-Offshore Seismic Data: Implications for the Dimensions and Slip Behavior of the Seismogenic Zone

Dan Bassett[1], Stuart Henrys[1], Brook Tozer[1], Harm van Avendonk[2], Andrew Gase[3], Nathan Bangs[2], Shuichi Kodaira[4], David Okaya[5], Katie Jacobs[1], Rupert Sutherland[6], Hannu Seebeck[1], Dan Barker[1], Gou Fujie[4], Ryuta Arai[4], Anya Seaward[1], Kimi Mochizuki[7], Martha Savage[5], Tim Stern[5], and Thomas Luckie[5]

[1]GNS Science, Lower Hutt, New Zealand, [2]Institute for Geophysics, Jackson School of Geosciences, University of Texas at Austin, Austin, TX, USA, [3]Department of Geosciences, Boise State University, Boise, ID, USA, [4]Japan Agency for Marine-Earth Science and Technology, Yokohama, Japan, [5]University of Southern California, Los Angeles, CA, USA, [6]School of Geography, Environment and Earth Sciences, Victoria University of Wellington, Lower Hutt, NZ, [7]Earthquake Research Institute (ERI), University of Tokyo, Tokyo, Japan

Key Points:

- Four decades of controlled-source seismic data constrain a high-resolution, regional P-wave velocity model of the Hikurangi subduction zone
- Spatial variability in wavespeeds reflect the tectonic evolution and distribution of geological terranes in the overthrusting plate
- The position of the crustal backstop is highly variable and may drive differences in the width and updip extent of frictional locking

Supporting Information:

Supporting Information may be found in the online version of this article.

Correspondence to:

D. Bassett,
d.bassett@gns.cri.nz

Citation:

Bassett, D., Henrys, S., Tozer, B., van Avendonk, H., Gase, A., Bangs, N., et al. (2025). Crustal structure of the Hikurangi subduction zone revealed by four decades of Onshore-Offshore seismic data: Implications for the dimensions and slip behavior of the seismogenic zone. *Journal of Geophysical Research: Solid Earth*, *130*, e2024JB030268. https://doi.org/10.1029/2024JB030268

Received 1 SEP 2024
Accepted 9 JAN 2025

Author Contributions:

Conceptualization: Dan Bassett, Stuart Henrys
Data curation: Dan Bassett, Stuart Henrys, Harm van Avendonk, Andrew Gase, Nathan Bangs, Shuichi Kodaira, David Okaya, Katie Jacobs, Rupert Sutherland, Dan Barker, Gou Fujie, Ryuta Arai, Anya Seaward, Kimi Mochizuki, Martha Savage, Tim Stern, Thomas Luckie
Formal analysis: Dan Bassett, Brook Tozer, Harm van Avendonk,

Abstract

Four decades of seismic reflection, onshore-offshore and ocean-bottom seismic data are integrated to constrain a high-resolution 3-D P-wave velocity model of the Hikurangi subduction zone. Our model shows wavespeeds in the offshore forearc to be 0.5–1 km/s higher in south Hikurangi than in the central and northern segments ($V_P \leq 4.5$ km/s). Correlation with onshore geology and seismic reflection data sets suggest wavespeed variability in the overthrusting plate reflects the spatial distribution of Late Jurassic basement terranes. The crustal backstop is 25–35 km from the deformation front in south Hikurangi, but this distance abruptly increases to ∼105 km near Cape Turnagain. This change in backstop position coincides with the southern extent of shallow slow-slip, most of which occurs updip of the backstop along the central and northern margin. These relationships suggest the crustal backstop may impact the down-dip extent of shallow conditional stability on the megathrust and imply a high likelihood of near/trench-breaching rupture in south Hikurangi. North of Cape Turnagain, the more landward position of the backstop, in conjunction with a possible reduction in the depth of the brittle ductile transition, reduces the down-dip width of frictional locking between the southern (∼100 km) and central Hikurangi margin by up-to 50%. Abrupt transitions in overthrusting plate structure are resolved near Cook Strait, Gisborne and across the northern Raukumara Peninsula, and appear related to tectonic inheritance and the evolution of the Hikurangi margin. Extremely low forearc wavespeeds resolved north of Gisborne played a key role in producing long durations of long-period earthquake ground motions.

Plain Language Summary

Some subduction zones produce the largest earthquakes and tsunamis on Earth, while others slip freely. New Zealand's Hikurangi subduction zone exhibits profound differences in slip-behavior, transitioning from a region of strong fault locking in the south, to a region where the fault slips episodically in slow earthquakes further north. To understand what factors impact subduction zone slip behavior, we have integrated over 4 decades of seismic data to construct a high-resolution, 3-D image of the Hikurangi subduction zone. This image shows that relative to north Hikurangi, seismic wavespeeds in south Hikurangi are faster, and the region of fast wavespeeds extends further offshore toward the subduction trench. Correlations with onshore geology and seismic images suggest these changes likely reflect differences in the offshore (updip) extent of basement rocks within the overriding plate. We suggest the distribution of basement rocks overlying the subduction interface influences the strength and distribution of fault locking, and the offshore extension of rigid basement rocks in south Hikurangi may enable earthquakes to rupture further offshore. Wavespeed differences in the overthrusting plate also impact durations of earthquake ground shaking. Our results reinforce the importance of crustal-scale architecture in modulating earthquake and tsunami hazard at subduction zones.

1. Introduction

The largest earthquakes on Earth take place on the megathrust of subduction zones where the shallow trajectory of subducting plates and the depression of isotherms provide wide zones over which seismic processes can occur.

Andrew Gase, Nathan Bangs, Dan Barker, Gou Fujie
Funding acquisition: Stuart Henrys, Harm van Avendonk, Nathan Bangs, Shuichi Kodaira, David Okaya, Kimi Mochizuki, Martha Savage, Tim Stern
Investigation: Dan Bassett, Stuart Henrys, Brook Tozer, Rupert Sutherland, Hannu Seebeck, Dan Barker, Gou Fujie, Ryuta Arai, Kimi Mochizuki
Methodology: Dan Bassett, Stuart Henrys, Harm van Avendonk
Project administration: Stuart Henrys, Harm van Avendonk, Nathan Bangs, Shuichi Kodaira, David Okaya, Katie Jacobs, Dan Barker, Gou Fujie, Anya Seaward, Kimi Mochizuki, Martha Savage, Tim Stern
Software: Harm van Avendonk
Validation: Dan Bassett
Writing – original draft: Dan Bassett
Writing – review & editing: Dan Bassett, Stuart Henrys, Brook Tozer, Harm van Avendonk, Andrew Gase, Nathan Bangs, Shuichi Kodaira, David Okaya, Rupert Sutherland, Hannu Seebeck, Ryuta Arai, Martha Savage, Tim Stern

The geological architecture of the overthrusting and subducting plates have long been shown to play key roles in modulating the rupture area, slip-distribution and magnitude of earthquakes (Bassett, Sandwell, et al., 2016; Kelleher & McCann, 1976; Robinson et al., 2006; Wang & Bilek, 2011), and the proximity of large co-seismic slip to densely populated coastal regions or deep-sea trenches (Byrne et al., 1988, 1993; Hyndman & Wang, 1995; Oleskevich et al., 1999; Sallarès & Ranero, 2019). More recently, constraints on geological architecture have also been shown to play a key role in subduction zone monitoring and hazard assessment, with accurate knowledge of the elastic structure improving earthquake hypocenter determination, inversions of geodetic data for fault slip (Williams & Wallace, 2018), and numerical simulations of earthquakes, ground motions and tsunamis (e.g., Aniko Wirp et al., 2021; Ulrich et al., 2022).

Obtaining high-resolution constraints on crustal structure over scales comparable to the rupture area of the largest earthquakes (~50,000–250,000 km^2) is, however, a challenge. Offshore seismic transects consisting of energy recorded by ocean-bottom seismometers and/or hydrophone streamers from thousands of closely spaced energy sources routinely provide the dense distribution of raypaths necessary for high-resolution imaging (spatial resolution 0.1–10 km); however, these images are typically 2-D and the acquisition geometry often limits refracted raypaths to <25 km depth (e.g., Arai et al., 2024; Gase et al., 2021; Kamei et al., 2012). Regional 3-D images are routinely generated using seismic energy recorded by seismometers from naturally occurring earthquakes; however, the sparsity of sources and receivers in these models, and in many cases the absence of offshore seismometers, often limits spatial resolution to 30–50 km horizontally and ~10 km in depth (e.g., Eberhart-Phillips et al., 2017; Liu & Zhao, 2018). In SW Japan, we have demonstrated how these limitations can be overcome via the integration of dense marine-geophysical data sets recorded onshore and offshore (Arnulf et al., 2022; Bassett, Arnulf, Kodaira, et al., 2022).

The Hikurangi margin, New Zealand, is one of the most extensively studied subduction zones on Earth. The anomalous thickness of the subducting Hikurangi Plateau has resulted in the forearc becoming subaerial at shallower megathrust depths (~12 km) and greater proximity to the trench relative to most other subduction zones (Litchfield et al., 2007; Nicol et al., 2007). This configuration has enabled terrestrial geodetic observations to reveal significant along-strike differences in megathrust slip behavior over an unusually large range of interface depths (Wallace, 2020; Wallace & Beavan, 2010; Wallace et al., 2004, 2012b, 2016). These data show the northern and central segment of the Hikurangi margin are characterized by weak interseismic locking and reveal the occurrence of shallow (<15 km depth), frequent (every 1–2 years), short-duration (several weeks to months) slow-slip events (SSEs) (Wallace et al., 2012b, 2016). The southern Hikurangi margin, by contrast, is characterized by strong interseismic locking to ~30–40 km depth, an abrupt reduction in the occurrence of shallow SSEs, and the occurrence of deep (>25 km), infrequent (5+ years) and long-lived (1–2 years) SSEs beneath Kāpiti and Manawatū (Wallace, Beavan, et al., 2012). The abrupt and well-documented transition in slip behavior between the southern and central segments, and the accessibility of shallow SSEs regions along the northern Hikurangi margin to geophysical imaging and ocean-drilling, has motivated IODP drilling and a wide-range of multidisciplinary field experiments aimed at resolving how the physical properties of subduction zones impact fault slip behavior (e.g., Bangs et al., 2023; Barnes et al., 2020; Chesley et al., 2021; Gase et al., 2021; Heise et al., 2023; Henrys et al., 2013; Wallace et al., 2016).

In this study, we integrate >40 years of seismic data recorded both onshore and offshore to construct a high-resolution 3-D seismic velocity model for the Hikurangi margin. We analyze this model to consider how crustal scale architecture may contribute to spatial variability in megathrust slip behavior.

2. Present Tectonic Setting

The Hikurangi margin accommodates westward subduction of the Hikurangi Plateau at rates of ~20–60 mm/year (DeMets et al., 2010; Mortimer & Parkinson, 1996). The Hikurangi Plateau is 11 ± 1 km thick beneath the Southern Plateau High (Figure 1) and reduces in thickness from south-to-north by 3–4 km across a NW-SE trending bathymetric scarp (shown as 3.25 km contour in Figure 1) resulting in a thickness of 7 ± 1 km beneath the Northern Volcanic Region (Bassett et al., 2023; Gase et al., 2021; Mochizuki et al., 2019). The Plateau is thought to have formed as part of a larger Hikurangi-Manihiki-Ontong Java Plateau (Coffin & Eldholm, 1994), with dredge samples and scientific drilling showing the Plateau sequence to consist of 96–118 Ma tholeiitic basaltic basement (Hoernle et al., 2010) overlain by Cretaceous clastic sedimentary rocks and Late Cretaceous to Early Oligocene chalks and mudstones (Barnes et al., 2020; Davy et al., 2008). Seamounts of alkali basalt

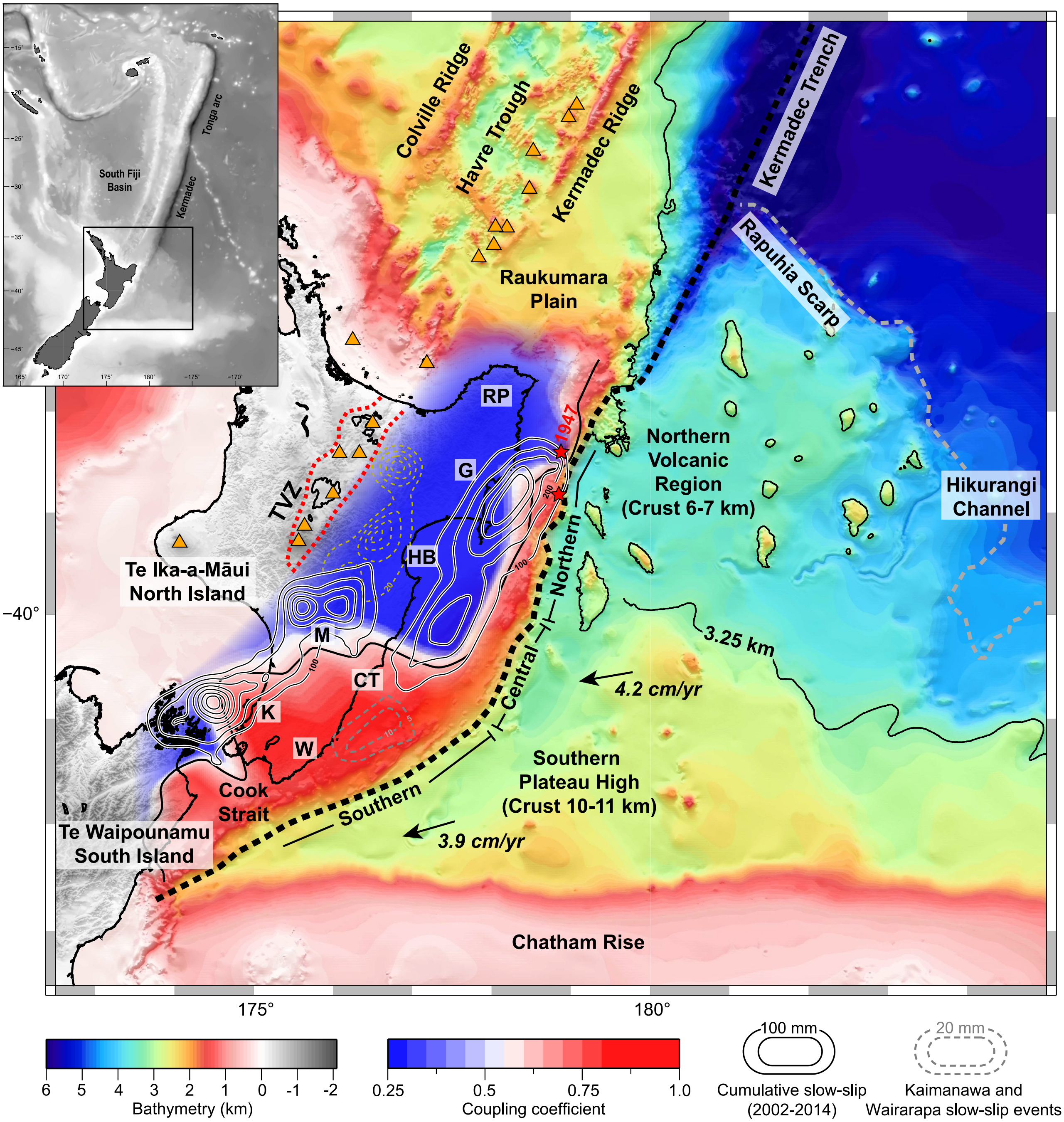

Figure 1. **Tectonic setting** of the Hikurangi subduction zone, New Zealand. Background color shows bathymetry (Mitchell et al., 2012) and interseismic coupling on the subduction interface (Wallace, Barnes, et al., 2012). Solid contours show cumulative slow-slip (2002–2014) (Wallace, 2020; Wallace, Beavan, et al., 2012). Dashed contours show two smaller SSEs offshore Wairarapa and beneath the Kaimanawa Ranges (Wallace and Eberhart-Phillips, 2013; Wallace, Barnes, et al., 2012). Red stars mark tsunami earthquakes in 1947 (Doser & Webb, 2003). Black contour offshore (3.25 km) marks the bathymetric and crustal thickness transition between the southern (10–11 km) and northern (6–7 km) Hikurangi Plateau (Bassett et al., 2023). Arrows indicate the azimuth and rate of plate convergence between the Pacific and Australian plates (DeMets et al., 2010). Orange Triangles mark active volcanoes. Annotation: CT = Cape Turnagain, HB = Hawke Bay, G = Gisborne, TVZ = Taupo Volcanic Zone, RP = Raukumara Peninsula, W = Wairarapa, K = Kāpiti, M = Manawatū.

composition (52–99 Ma), younger Cenozoic intraplate volcanoes and late-stage Pliocene volcanics are prominent features of the Hikurangi Plateau (Barnes et al., 2010; Gase et al., 2024; Hoernle et al., 2010; Timm et al., 2010). Seismic and electromagnetic data sets show the internal structure of seamounts to consist of a high-velocity and resistive core embedded within a larger, lower-velocity and more conductive matrix (Arai et al., 2020; Bassett et al., 2023; Chesley et al., 2021; Gase et al., 2021, 2023b). The bathymetric expression of seamounts progressively increases from south-to-north in response to the sedimentary cover sequence decreasing in thickness from 4 to 5 km offshore Cook Strait and Wairarapa, to ~0.5–1.5 km thickness along the northern Hikurangi margin (e.g., Barnes et al., 2010; Gase et al., 2022; Gase et al., 2024; Lewis et al., 1998). The subduction of seamounts along the north Hikurangi margin has been linked with large debris avalanches offshore Poverty Bay and Ruatoria (Collot et al., 1996, 2001; Lewis et al., 1998, 2004; Pedley et al., 2010), locally enhanced fluid flux via the subduction of porous and altered volcanic matrices and the entrainment of fluid-rich sediment lenses (Bangs et al., 2023; Barker et al., 2018; Bell et al., 2010; Chesley et al., 2023; Gase et al., 2023a), and heterogeneity in the distribution of fluids in the overthrusting plate in response to the enhanced loading and stress shadows that form above the leading and trailing flanks of subducting seamounts, respectively (Chesley et al., 2021; Sun et al., 2020). Rough crust subduction and the resulting heterogeneity in the geometry, lithology and physical properties of the megathrust have been proposed to promote the occurrence of shallow slow-slip along the north Hikurangi margin and the occurrence of two tsunami earthquakes offshore Gisborne and Tolaga Bay in 1947 (e.g., Bangs et al., 2023; Barker et al., 2018; Barnes et al., 2020; Bell et al., 2014; Chesley et al., 2021; Shreedharan et al., 2023).

The composition, structure and morphology of the forearc wedge varies in response to along-strike variability in subduction inputs and the geological architecture of the overthrusting plate. The Late-Cenozoic accretionary wedge varies along-strike from a relatively narrow (~30 km wide) prism of hemipelagic turbidites and the pelagic plateau cover sequence offshore Wairarapa (Barnes et al., 2010; Bland et al., 2015; McArthur et al., 2020; Stevens et al., 2024), transitioning to a wide (65–70 km) low-taper accretionary prism of similar composition through the central portion of the margin (Barnes et al., 2010; Gase et al., 2022; Ghisetti et al., 2016; Plaza-Faverola et al., 2016). Offshore and north of Hawke Bay, the thickness of trench-fill turbidites, and particularly the pelagic plateau cover sequence, diminish significantly (<0.5 s twtt) and the morphology of the outer-wedge changes to a steeper and narrower frontal wedge, with a highly deformed pre-subduction sequence of Cretaceous and Paleogene rocks interpreted to overlie the megathrust within 10–30 km of the deformation front (Barnes et al., 2010, 2020; Gase et al., 2021). These rocks are similar in age and composition to the Torlesse 'basement' that cores the inner-forearc, but the latter is distinguished by a higher metamorphic grade and degree of induration associated with accretion to the Gondwana forearc (Bland et al., 2015; Moore & Speden, 1984).

The inner-forearc is composed of the Torlesse composite terrane, which is exposed in the coastal foothills of Wairarapa and along the Axial Ranges extending the length of the margin (Heron, 2014; Mortimer, 2004). Along-strike differences in the constituents of the Torlesse composite terrane (Reyners & Eberhart-Phillips, 2009) and the position of the crustal backstop (Bassett, Arnulf, Henrys, et al., 2022) have been proposed to influence upper-plate permeability and interseismic coupling, and the down-dip extent of shallow conditional stability, respectively. The state of stress in the upper-plate varies from long-term transpression in south Hikurangi to upper-plate extension through the central and northern margin and is proposed to impact interseismic coupling and the depth distribution of SSEs via the impact of upper-plate stress on vertical structural permeability, fluid pressure and the depth to the frictional-to-viscous transition (Fagereng & Ellis, 2009; Wallace, Fagereng, & Ellis, 2012). Relative to the southern margin, seismic and magnetotelluric observations show the northern Hikurangi forearc to be characterized by lower V_P, higher V_P/V_S, high attenuation and low resistivity (Bassett et al., 2014; Chow et al., 2022; Eberhart-Phillips & Bannister, 2015; Eberhart-Phillips et al., 2017; Heise et al., 2017, 2023). These observations have been interpreted to suggest larger volumes of fluids in the overthrusting plate and potentially differences in stress-state, which may be consistent with geochemical data revealing enhanced upper-plate permeability via a factor of 3 reduction in fluid residence times relative to the locked southern Hikurangi margin (Barnes et al., 2019; Reyes et al., 2010). Arc volcanism is largely confined to the Taupo Volcanic Zone (TVZ) although it also occurs further west at Mount Taranaki (Price et al., 2005; Wilson et al., 1995). There is no volcanic arc along the southern Hikurangi margin, which has experienced persistent contraction and shortening during the last ~5 Ma (Jiao et al., 2017; Nicol et al., 2007).

While no historic great (Mw ≥ 8.0) earthquakes have occurred along the Hikurangi margin, abrupt coastal deformation and tsunami deposits have been used to identify 10 possible subduction earthquakes over the past 7,000 years (Clark et al., 2019; Pizer et al., 2021). The deeply locked southern Hikurangi margin has ruptured in Mw > 8.0 earthquakes every 335–655 years, producing four large megathrust earthquakes in the last 2000 years (Clark et al., 2019; Pizer et al., 2021). Coastal subsidence in central Hikurangi requires that at least a subset of the identified earthquakes occur on the plate interface, raising the possibility of different modes of slip-behavior with portions of the central Hikurangi megathrust capable of failing as SSEs or in large earthquakes (Clark et al., 2019; Delano et al., 2023; Pizer et al., 2023). The largest subduction thrust earthquakes in the historical record occurred offshore Gisborne where two M ∼ 7 tsunami earthquakes ruptured the shallow, mostly creeping sections of the northern-Hikurangi margin in 1947 (Figure 1) (Bell et al., 2014; Doser & Webb, 2003).

3. Data and Methods

3.1. Geophysical Data

We have compiled a data set of onshore-offshore receiver-gathers that has swelled for over four decades as seismic energy from 186 seismic profiles offshore was passively recorded by 338 temporary and permanent onshore seismometers (Figure 2). We integrate these data with inline and offline OBS data from three marine seismic experiments, land explosion data from two experiments and shallow seismic velocity constraints from seismic reflection surveying to constrain a 3D seismic velocity model for the Hikurangi margin.

The seismic data set extends back to 1991 when the Hikurangi Margin Seismic Experiment (HMSE) acquired wide-angle seismic data from 6 explosions (2 offshore, 4 onshore) recorded by 86 seismometers deployed along a 300 km onshore transect extending from Cape Palliser to Cape Kidnappers (Figure 2) (Chadwick, 1997). The first onshore-offshore data set was acquired in 1994 when the R/V *Explora* acquired 394 km of marine seismic data between Cook Strait and Christchurch. This survey coincided with the PANDA deployment of 24 onshore seismometers, with seismic energy from the 71-L seismic source well recorded onshore. In 2001, the NIGHT experiment acquired an onshore-offshore transect across the central North Island, consisting of 15 OBS deployments along a 300 km long offshore seismic reflection line (Henrys, 2003). Onshore, 288 NIGHT temporary seismometers recorded energy from the MCS seismic source and from 14 land explosions (Stratford & Stern, 2006). In 2005 and 2007, grids of seismic reflection data offshore the central/north Hikurangi margin (05CM - ∼2,800 line km) and within Raukumara Basin (RAU07–1,128 line km) were acquired primarily for petroleum exploration; however, wide-angle seismic data were recorded by temporary deployments of onshore seismometers and by the nationwide GeoNet network (Barker et al., 2009; Bassett et al., 2010; Sutherland et al., 2009). OBS data were acquired across Raukumara Basin in 2007 by R/V *Sonne* during the MANGO experiment (Bassett, Kopp, et al., 2016; Scherwath et al., 2010). In 2009, the multi-national SAHKE experiment leveraged the offshore acquisition of the PEG09 industry seismic reflection data set (∼3,200 line km) and complemented this via the deployment of 67 temporary seismometers (Henrys et al., 2013, 2020). These seismometers were first deployed in a regional array to record earthquakes and PEG09 seismic sources, before being redeployed to record offshore shots from the double-sided onshore-offshore SAHKE transect and three transects offshore Wairarapa (PEG23-25) and within Wanganui Basin (SAHKE3). Inline and offline shots from each of these lines were recorded by 20 OBSs, with most (16) of these deployments positioned above the shallow megathrust along the eastern limb of the SAHKE transect (Henrys et al., 2013). Phase two of SAHKE reoccupied the onshore transect with 871 seismometers, which recorded seismic energy from 12 land explosion sources. In 2014, WesternGeco acquired 5,242 km of seismic reflection data across the central Hikurangi margin during the PEG14 survey, with shots widely recorded onshore by the nationwide GeoNet network. Finally, in 2017 the multi-national SHIRE experiment acquired a margin-wide grid of seismic reflection and refraction data, with 5,489 km of seismic refection data acquired using a 108 L source and 12.75 km streamer by *R/V M.G. Langseth*, and *R/V Tangaroa* deploying 114 OBSs along 5 transects (Figure 2). Onshore-offshore data were recorded by a temporary array of 89 seismometers around Raukumara Peninsula, 46 of which were deployed in a distributed array, with the remaining 43 deployed in a 2D coast-coast transect. Onshore offshore data were also recorded by the BEACON temporary deployment of 22 broadband seismometers south of Hawke Bay (Kaneko & Chow, 2017) and by GeoNet seismometers. Phase 2 of SHIRE reoccupied the coast-to-coast transect with 583 short-period seismometers, which recorded seismic energy from five onshore explosive sources.

Controlled-source receiver gathers (Figures 3 and 4) were processed using GLOBE Claritas and a simple processing sequence consisting of a Zero-phase Butterworth frequency filter with ramps at 2–4 and 10–20 Hz, trace amplitude balancing and resampling at 5 ms. Processed receiver gathers were then interpreted using Seisware. Rather than interpreting receiver-gathers following a line-by-line approach, Seisware allowed all receiver-gathers for a single seismometer to be loaded, viewed and interpreted simultaneously, enabling a more efficient, accurate and internally consistent volume-based method of travel-time interpretation.

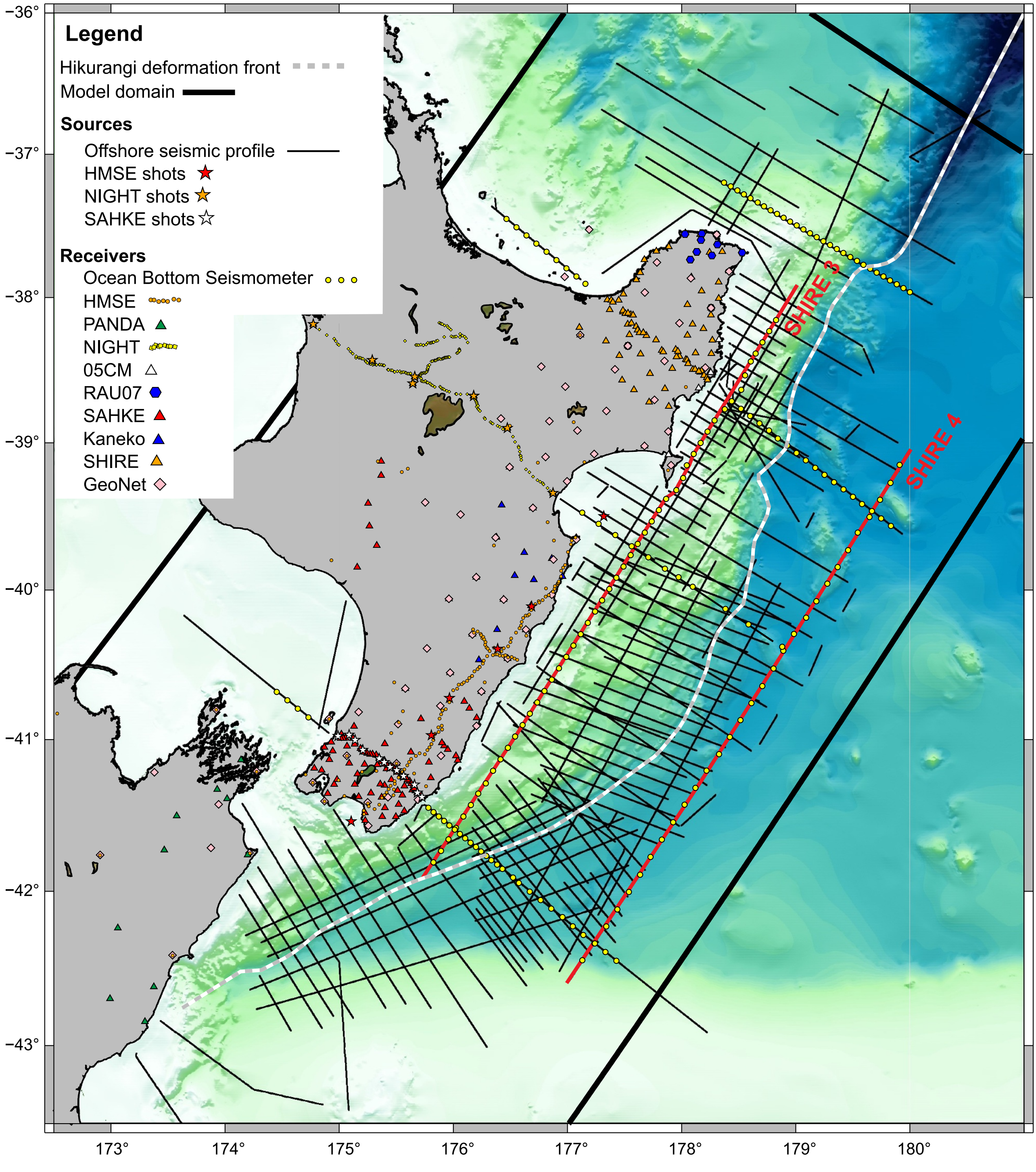

Figure 2. Geophysical Data. Wide-angle seismic data acquired along the Hikurangi margin. Solid black lines offshore show seismic reflection profiles. The onshore arrival of seismic energy from each profile was recorded by permanent and temporary deployments of seismometers (color coded in Legend). Stars show the location of onshore shots associated with the HMSE, NIGHT, and SAHKE experiments. Yellow dots offshore show temporary deployments of Ocean Bottom Seismometers. Thick black line shows the extent of the 3D tomographic inversion model domain.

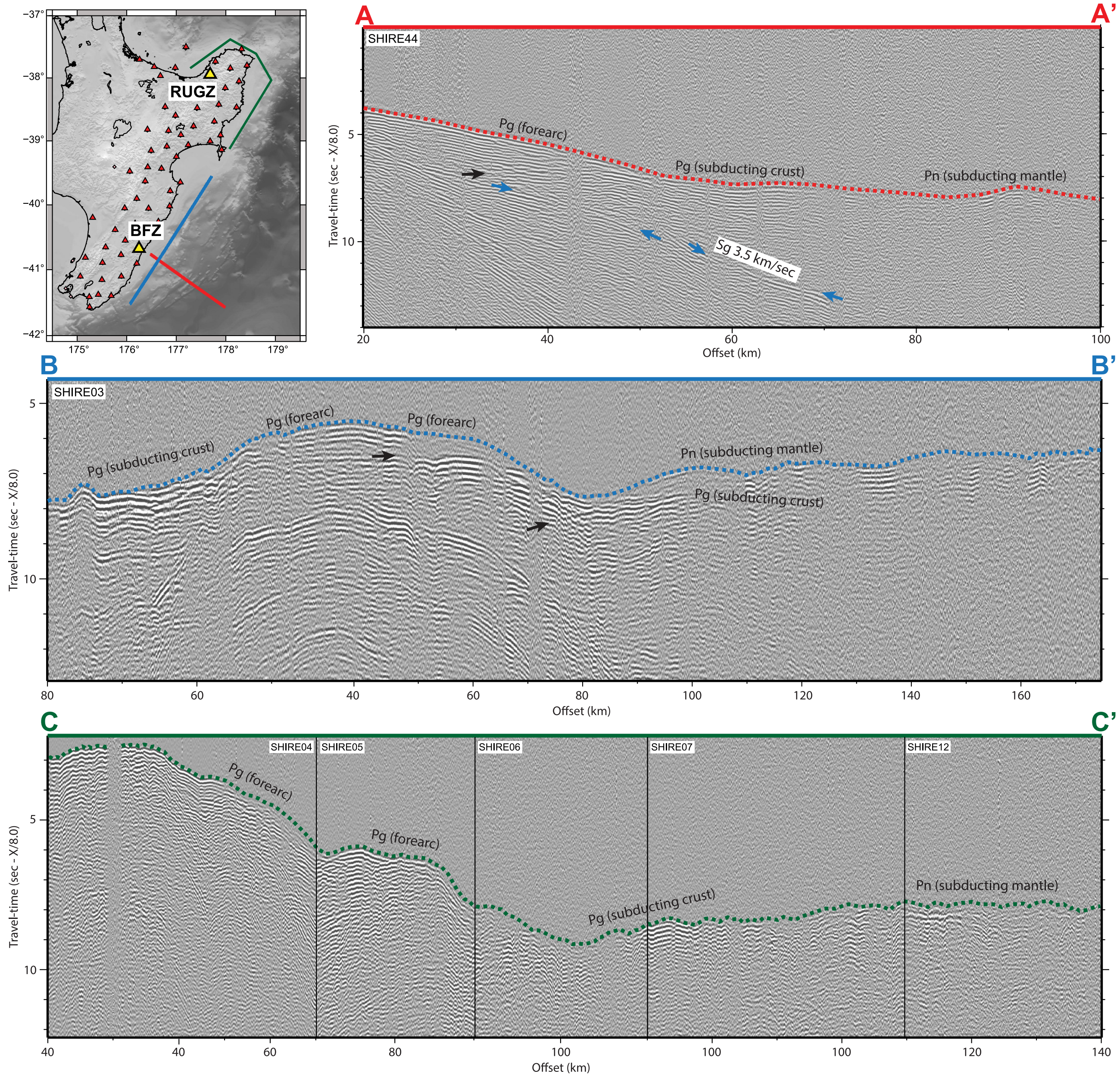

Figure 3. Onshore-offshore wide-angle seismic data. (a) Profile A-A' shows seismic energy from shots along the dip-parallel transect SHIRE44 (red in inset map) recorded onshore Wairarapa at GeoNet seismometer BFZ. Seismic data are reduced to 8 km/s. Colored dashed line shows interpreted first arrival with labels indicating interpreted phases. Black and Blue arrows mark wide-angle reflections and S-wave arrivals respectively. (b) Profile B-B' shows seismic energy recorded from the strike-parallel transect SHIRE03 by BFZ. (c) Profile C-C' is a composite gather showing seismic data recorded at RUGZ from 5 seismic lines extending around Raukumara Peninsula from the eastern Bay of Plenty to Māhia Peninsula.

The collective data set we have analyzed consists of 13,748 onshore-offshore receiver gathers (Figure 3), capturing airgun shots from 186 offshore seismic lines recorded by 338 onshore seismographs, from which we have made 4.35×10^6 first-arrival travel-time interpretations (Figures 5 and 6). The OBS data set (Figure 4) consists of 509 receiver gathers (174 deployments and 8 seismic lines), from which we have made a further 4.2×10^5 travel-time interpretations. The onshore-shot data set provides 2.5×10^3 travel-times from 24 onshore shots into 552 seismographs (Chadwick, 1997; Henrys et al., 2013; Stratford & Stern, 2006).

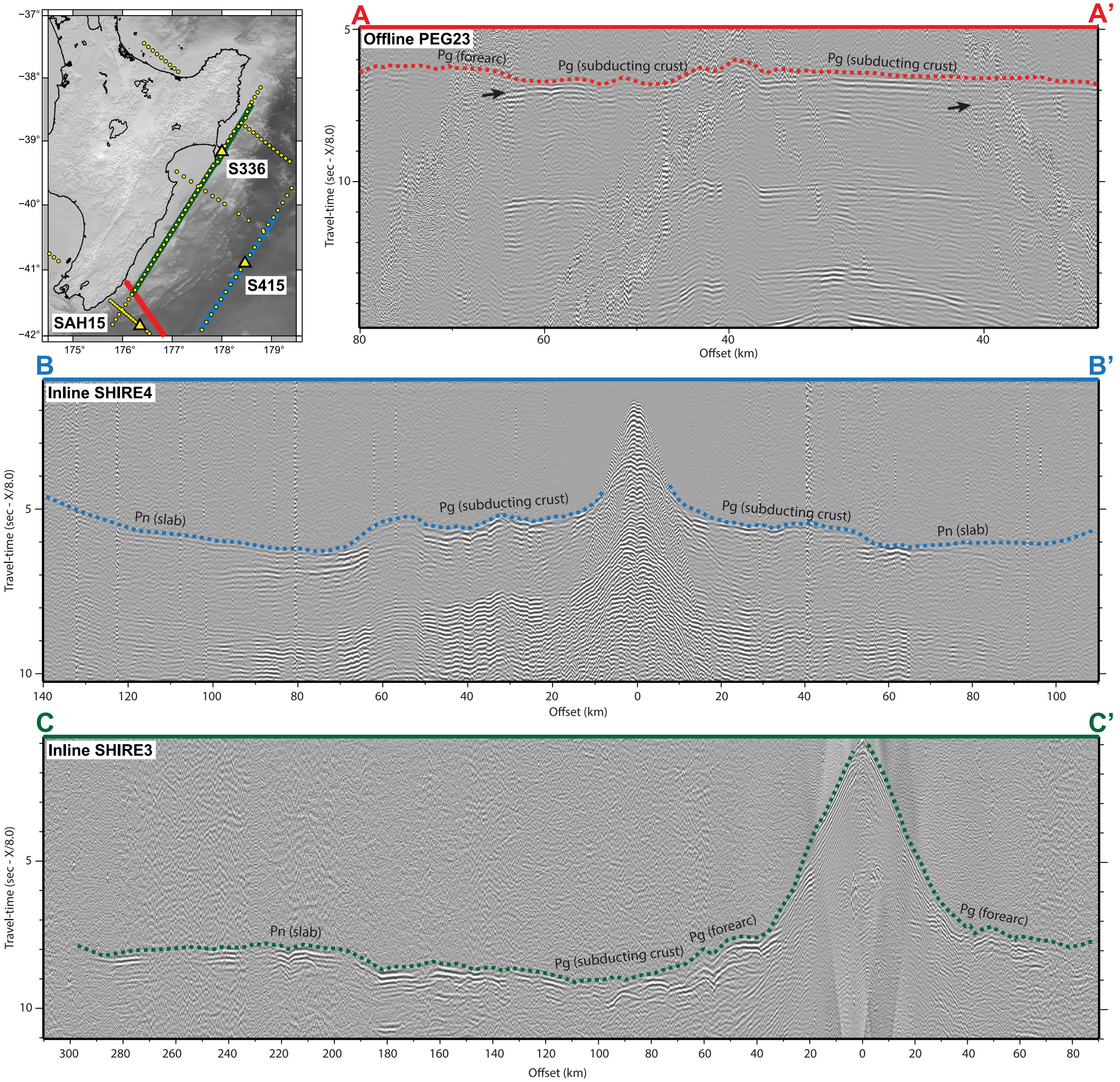

Figure 4. Ocean-Bottom wide-angle seismic data. (a) Profile A-A’ shows offline seismic data from shots along transect PEG23 (red in inset map) recorded along the SAHKE transect by OBS SAH15. Seismic data are reduced to 8 km/s. Colored dashed line shows interpreted first arrivals with labels indicating interpreted phases. Black arrows mark wide-angle reflections. (b) Profile B-B’ shows inline seismic data recorded along the Hikurangi Plateau by OBS S415 from the strike-parallel transect SHIRE 4. (c) Profile C-C’ shows inline seismic data recorded along the Hikurangi forearc by OBS S336 from the strike-parallel transect SHIRE 3.

Figures 5a and 5b shows the ray coverage of the onshore-offshore, OBS and onshore-shot data sets. Figure 5c shows the distribution of source-receiver offsets, revealing that 90% of the onshore-offshore data set has offsets ≥50 km and 75% has offsets ≥75 km. This distribution of source-receiver offsets is not well suited to resolving shallow (within ~5 km of the seabed) seismic velocity structure offshore, with the trade-off between shallow and deep seismic velocity structure impacting the reliability of crustal scale imaging at both depths if the near-surface is not constrained. In SW Japan, these constraints were obtained from 5 regional OBS surveys (>850 OBS deployments) conducted by the Japan Agency for Marine-Earth Science and Technology, which collectively provide a dense 3D data set of short-offset, offshore raypaths spanning the full length and width of Nankai Trough (Bassett, Arnulf, Kodaira, et al., 2022). In this study, the available OBS data set is significantly smaller and

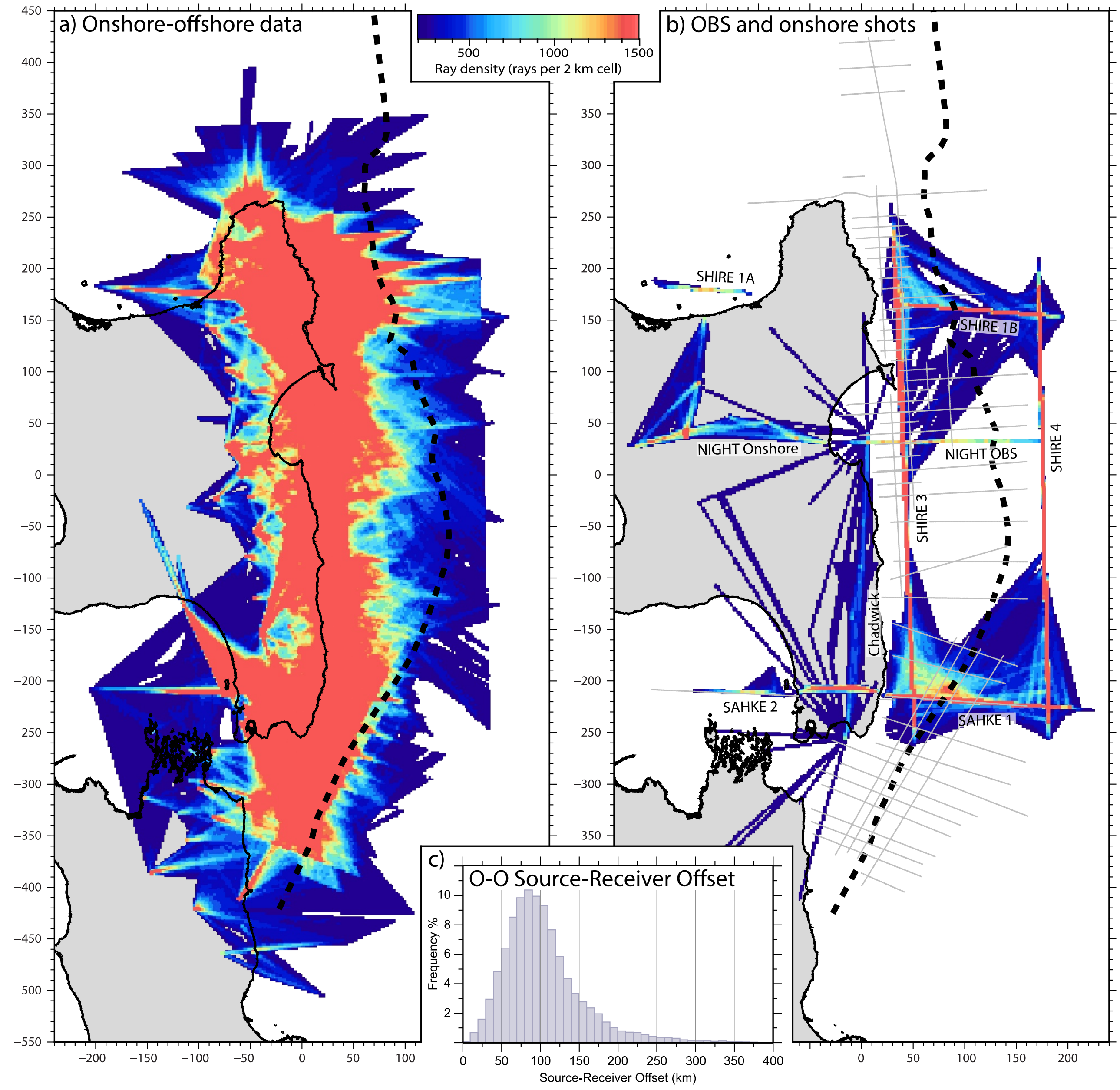

Figure 5. Ray density. (a) Ray density provided by onshore-offshore seismic data. Ray density is calculated as the number of rays within a 2 km search radius. Dashed black line marks the deformation front. (b) Ray density provided by OBS and onshore shots. Gray lines offshore show seismic lines along which constraints on shallow seismic velocities were incorporated into our starting model. (c) Source receiver offset distribution for the onshore-offshore data set. Cross-sections and depth slices of ray density are provided in supplementary information (Figure S2 in Supporting Information S1).

predominantly 2-D in nature, with offline OBS data only recorded within small wedges in south Hikurangi, north Hikurangi and Wanganui Basin (Figure 5b). We have therefore constrained the shallow-seismic velocity structure offshore by compiling, processing and gridding near-surface interval velocity data derived from the processing of 67 offshore seismic lines (gray lines Figure 5b).

3.2. Starting Model Construction

Our background starting model is version 2.3 of the nationwide seismic velocity model of Eberhart-Phillips et al. (2022). This model has been refined offshore via the incorporation of shallow seismic velocity

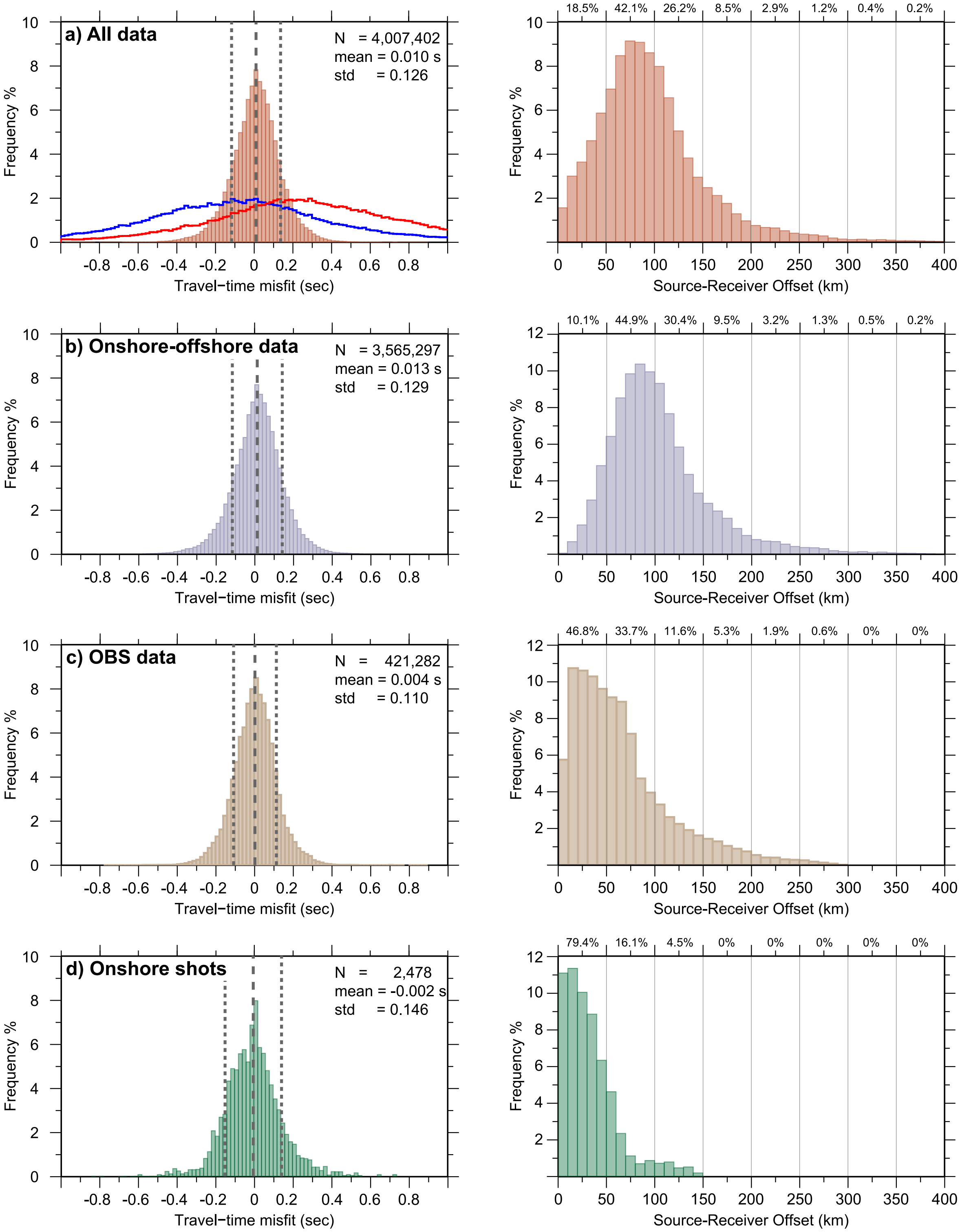

Figure 6. Pick statistics and misfit statistics. (a) Left panel shows the distribution of travel-time misfits for all data after performing our 3D tomographic inversion. Dashed and dotted lines show the mean and standard deviation. Red and Blue lines show the misfit distribution when our data set is compared with travel-times calculated through regional 3D velocity models derived from earthquake (Eberhart-Phillips et al., 2017) and adjoint (Chow et al., 2022) tomography respectively. Right panel shows the distribution of source-receiver offsets, with the proportion of data within each 50 km wide bin provided above. (b)–(d) As in (a), but shown discreetly for (b) Onshore-offshore, (c) OBS and (d) Onshore shot data.

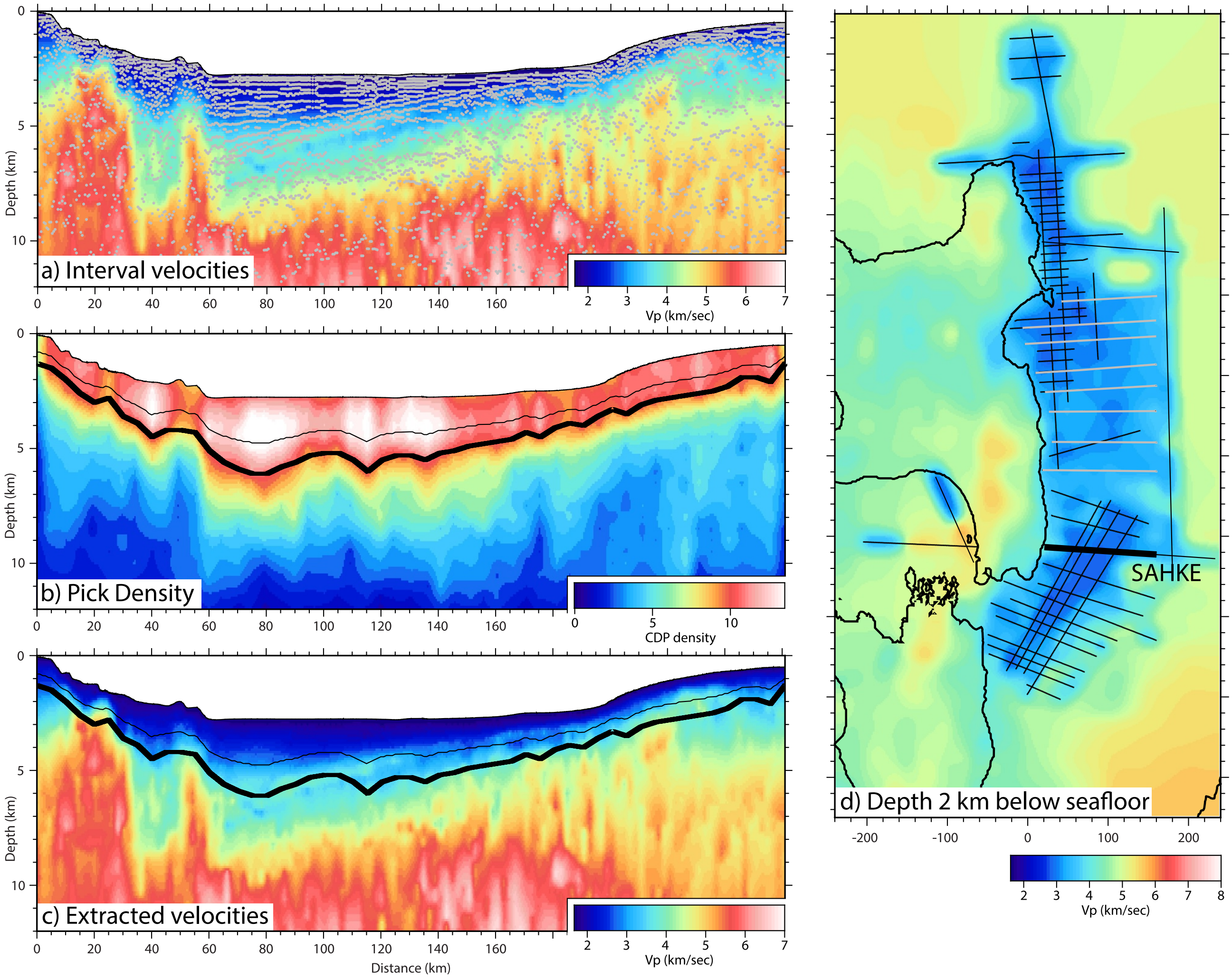

Figure 7. **Shallow velocity constraints from MCS data.** (a) Interval velocities derived from the processing of seismic reflection data along the SAHKE profile (bold in map). Gray dots illustrate the spatial distribution of velocity determinations. (b) Density of velocity determinations. Density is calculated as the number of picks within a 5 km horizontal and 2 km vertical search radius. Thick black line marks the maximum depth at which interval velocities are considered well determined based on a threshold comparing pick density with subseafloor depth. (c) Interval velocities with the density versus depth threshold illustrating what velocities will be incorporated into our starting velocity model. (d) Depth slice taken 2 km below the seafloor showing the distribution of shallow constraints from MCS data (black profiles) and the resulting velocity distribution after gridding and incorporation into the background regional velocity structure. Additional cross-sections and depth slices of our starting model are provided in supplementary information (Figure S1 in Supporting Information S1).

constraints from 67 seismic reflection profiles and crustal scale constraints on seismic velocities and the thickness of the Hikurangi Plateau from 2D seismic refraction models.

The reliability of interval velocity data derived along seismic reflection profiles is highly variable and is impacted by streamer-length relative to depth and the subsurface distribution of reflectors from which velocity picks can be made. Both parameters diminish with increasing depth and the deeper sections of most interval velocity models are either not well determined or are filled by interpolation (Figure 7a). To estimate what portions of interval velocity models are reliability determined, we analyze the spatial-density and standard-deviation of interval velocity picks (Figure 7b). For each position along a profile, we then define the maximum depth at which interval velocity picks are considered well-determined via a function comparing interval velocity pick density to sub-seafloor depth (Figure 7c), which is used to extract the interval velocities that will be incorporated into our starting model. Seismic velocity constraints along SHIRE MCS profiles (gray in Figure 7d) were derived by joint reflection/streamer-refraction tomography, enabling semblance grids to be used to define the maximum depth at which seismic velocities are well-determined (van Avendonk et al., 2023).

Interval velocities extracted from all profiles were converted to depth below the seafloor and integrated with crustal scale seismic velocity constraints from 2D wide-angle seismic velocity models from north Hikurangi (Gase et al., 2019, 2021), south Hikurangi (Mochizuki et al., 2019; Tozer et al., 2017) and two strike profiles traversing the full length of the Hikurangi margin landward (Bassett, Arnulf, Henrys, et al., 2022) and seaward (Bassett et al., 2023) of the deformation front, respectively. These data were then gridded every 500 m below seafloor, using a smoothing radius that increased linearly from 5 km (depth ≤5 km) to 50 km (depth ≥28 km), and horizontal (40 km) and vertical (2 km) ramps that defined the minimum distance over which newly incorporated seismic velocities would grade back into the background nationwide seismic velocity model. The mesh defining our velocity model has a horizontal node spacing of 2 km and a vertical node spacing of 500 m.

The final step in developing our starting model was to incorporate wide-angle seismic constraints on the Moho geometry of the Hikurangi Plateau. These constraints were incorporated by extracting the Moho geometry from two margin-normal (Gase et al., 2021; Mochizuki et al., 2019) and two margin-parallel (Bassett et al., 2022a, 2023) wide-angle transects and then gridding these data alongside a smoothed representation of deeper geometry (depth >28 km) of the subducting Plateau Moho that was estimated by adding 12 km to a smoothed version of the subduction interface model of Williams et al. (2013). The crust overlying this Moho was prescribed a velocity gradient increasing from 6 to 7.2 km/s over 10 km in depth and the underlying mantle was prescribed a velocity of 8.1 km/s.

Cross-sections and depth slices through our starting model are provided in Supplementary Information (Figure S1 in Supporting Information S1). Refining our starting model through the integration of seismic velocity constraints from MCS and wide-angle seismic data reduced the χ^2 misfit of our starting model to 14.5 and a root mean squared (RMS) error of 430 ms, compared to a χ^2 misfit of 40 and an RMS error of 791 ms for the unmodified nationwide tomographic model of Eberhart-Phillips et al. (2022). The sensitivity of results to our starting model was assessed via a Monte Carlo approach, which is described below.

3.3. First-Arrival Travel-Time Tomography and Resolution Testing

Travel-time tomography was carried out using a version of the algorithm originally developed by Van Avendonk et al. (2004), which has been fully parallelized and optimized for large computational problems (Arnulf et al., 2018). This algorithm uses a hybrid scheme of the shortest-path method (Moser, 1991) and ray-bending (Van Avendonk et al., 2001) for the forward calculation of synthetic travel-times. Weighted travel-time residuals are then back-propagated along ray-paths, with iterative model updates calculated by minimizing a least squares cost-function penalizing the misfit between observed and calculated travel-times and model roughness.

This algorithm has been modified further to enable shallow seismic velocity constraints from offshore MCS profiles to be preserved throughout our inversion of longer-offset, deeper penetrating onshore-offshore and OBS seismic data sets. This was achieved by adjusting the right-hand side of the vector used to damp model perturbations, so that model perturbations are damped toward our starting model in near-surface regions that are constrained by shallow seismic velocity models offshore and are damped toward zero in all other regions. In Figures 7b and 7c, the thin and thick solid black lines mark the depth range over which velocity perturbations grade from being damped toward shallow wavespeed constraints from MCS data, to being damped toward zero, respectively.

Model updates were performed on a grid that was progressively refined as χ^2 reduced from an initial horizontal discretization of 40–8 km for the final iterations when $\chi^2 \leq 1.2$. The vertical discretization of the model increased with depth from a node spacing of 500 m at depths ≤10 km, before increasing linearly to a discretization 3 km at 50 km depth. Horizontal and vertical extensions of ray-coverage progressively reduced with χ^2 from 20 to 5 km respectively for the initial stages of the inversion, and 6 and 2 km respectively for the final iterations.

Interpreted travel-times are down-sampled in shot domain to 200 m. Seismic data were then incorporated within two source-receiver offset bands, with an initial model constructed for all data with source-receiver offsets ≤70 km. This initial model took 14 iterations to achieve a χ^2 of 1.0, with a χ^2 reduction target of 30% for each iteration. This short-offset model then served as the starting model for an inversion of seismic data from all offsets, which took a further 14 iterations to converge on our final model. The final velocity model has a χ^2 misfit of 1.02 and an RMS error of 81 ms (Figure 6).

Spatial resolution was assessed by preforming checkerboard tests consisting of a 40 × 40 × 8 km checkerboard perturbation with a maximum amplitude of ±0.4 km/s (Figure 8). These tests show our model to be well

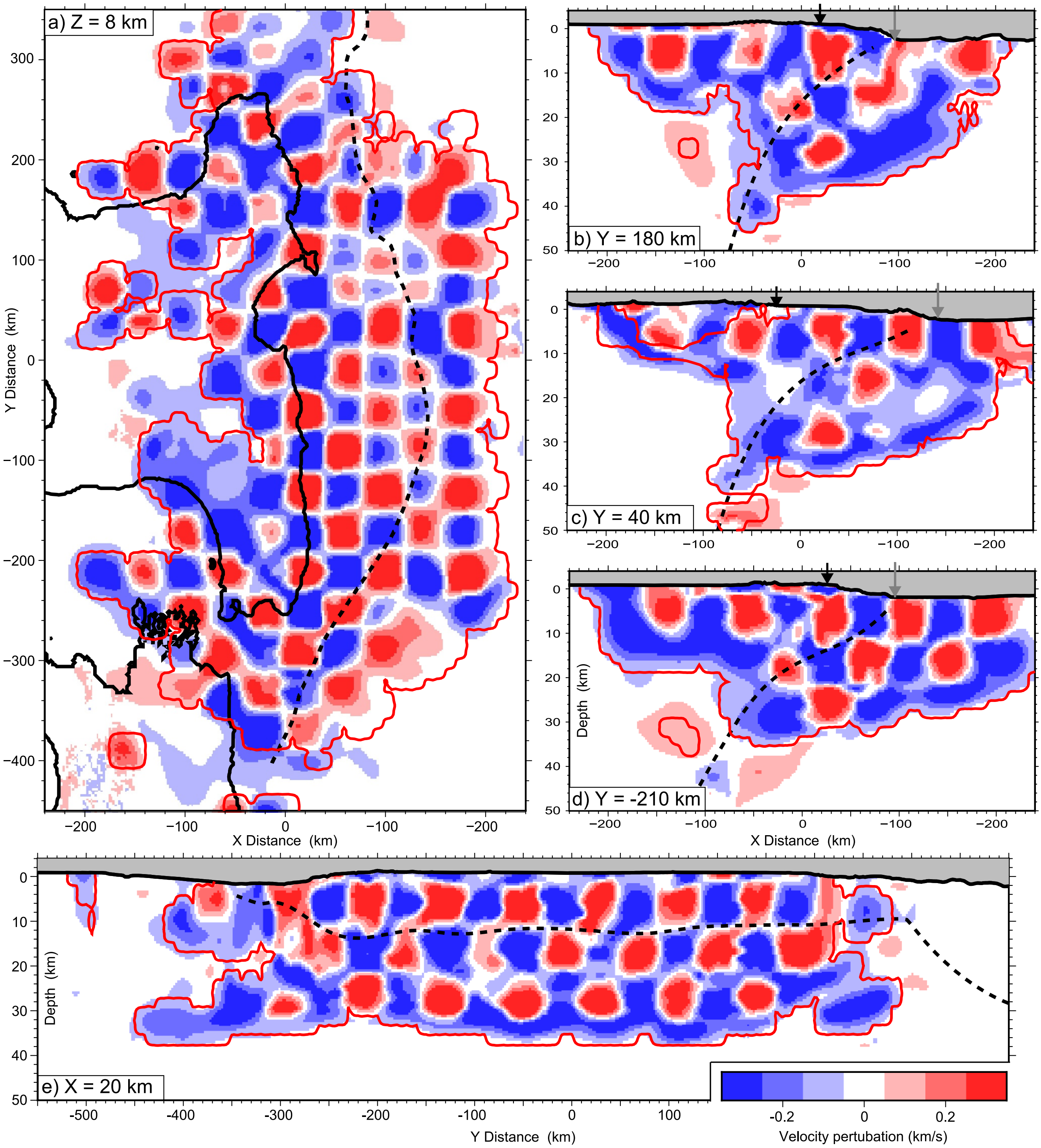

Figure 8. Checkerboard resolution test. (a) Depth slice showing checkerboard recovery at 8 km depth. The perturbation imposed was a 40 × 40 × 8 km P-wave velocity perturbation of ±0.4 km/s. Dashed black line marks the deformation front. Solid red line shows the extent of checkerboard recovery, which is used to illustrate the resolved region in cross-sections of model results (Figures 9 and 10). (b)–(d) *Y* slices showing checkerboard recovery down-dip at (b) $Y = 180$ km, (c) $Y = 40$ km and (d) $Y = -210$ km. Gray arrow marks the deformation front. Strongest recovery of the checkerboard pattern occurs within a triangular wedge centered near the coastline (marked by black arrow), which is consistent with where our onshore-offshore ray density is greatest and extends to greatest depth (Supplementary Figure S2 in Supporting Information S1). Dashed black line marks the geometry of the subduction interface (Williams et al., 2013). (e) *X* slice showing checkerboard recovery along strike at $X = 20$ km.

recovered above 25 km depth and locally in excess of 35 km. Strongest checkerboard recovery occurs within a 250–350 km wide triangular wedge, which is centered near the coastline (Black arrow in Figures 8b–8d) and extends down to ∼30 km depth. This recovery distribution is consistent with where our onshore-offshore data set has the highest ray density and where these rays reach their greatest depth (Supplementary Figure S2 in Supporting Information S1). The size of the imposed checker perturbation is close to the minimum wavelength that our data set can resolve on a regional basis, however, the distribution of raypaths is non-uniform and shorter-wavelength structure is readily resolved in regions of higher ray-density.

The sensitivity of results to our starting model and uncertainty in seismic velocities was estimated via a Monte Carlo approach. This consisted of applying random 30 × 30 × 8 km velocity perturbations of ±0.5 km/s to our starting model and then inverting our travel-time data set within a framework in which model damping, correlation-lengths and the χ^2 values at which inversion grid refinement occurs were all varied. We generated 100 models and Supplementary Figure S3 in Supporting Information S1 shows the standard deviation in velocities across this ensemble. This calculation shows the standard deviation in seismic velocities is typically ±0.15 km/s above 20 km depth and ±0.10 km/s in regions of high ray-density (Figure S2 in Supporting Information S1). Standard deviations are highest within the crust and mantle of the subducting Hikurangi Plateau, particularly at depths >20 km, which is consistent with the long offset of rays propagating through the deepest extents of the model and the inability of these rays to overcome trade-offs between crustal velocities, crustal thickness and wavespeeds in the underlying mantle. Monte Carlo results also reveal a halo of low standard deviations around the extent of ray-coverage and checkerboard recovery (red line in Figure S3 in Supporting Information S1). This halo reflects the long-wavelength and resulting similarity in model updates for the initial iterations of each inversion. These model updates minimize the influence of our stating model and the random perturbations imposed upon it. It follows that the primary factors leading to the variation in velocities where we have ray coverage is the model damping and regularization, and not our starting model.

4. Results

Figures 9 and 10 show margin-normal and margin-parallel slices through our 3-D P-wave seismic velocity model of the Hikurangi margin. In the overthrusting plate, our model reveals clear along-strike variability in the position of the crustal backstop and the distribution of low-velocity materials overlying the shallow megathrust. In the southern Hikurangi margin, low- wavespeeds ($V_P \leq 4.5$ km/s) in the outer-forearc are confined to a narrow region, with crustal rocks overlying the subduction interface within 30 km of the deformation front and making up the bulk of the onshore forearc (Figure 9g). Through the central Hikurangi margin, the lower taper of the backstop and outer-wedge, and the eastward migration of the deformation front significantly increases the distance to the crustal backstop to 90 km off Cape Turnagain and ∼100 km off Cape Kidnappers (Figures 9e and 9f). Here, thick (>5 km) basins of low velocity material ($V_P \leq 4.0$ km/s) persist in the near surface up to 50 km west of the coastline, with near surface crustal velocities ($V_P \geq 4.5$ km/s) only observed proximal to the axial ranges (Figure 9f). This margin architecture persists north of Māhia (Figure 9d), with an increase in wedge-taper reducing the distance to the backstop to ∼75 km. North of Gisborne (Figure 9c), the overthrusting plate exhibits an abrupt drop in wavespeeds, maintaining wavespeeds as low as 3.5 km/s to depths of ∼7 km offshore. This low-velocity wedge is up-to 120 km wide, 12 km deep and extends up-to 50 km onshore. Steep horizontal velocity gradients reveal the contrast in wavespeeds across Raukumara Peninsula, with the western half significantly faster than the low V_P wedge resolved further east and characterized almost exclusively by wavespeeds typical of consolidated crust or basement (4.5–7.2 km/s) (Figure 9c).

Figure 10d shows a strike-parallel slice near the coastline and reveals crustal iso-velocity contours ($V_P \geq 4.5$ km/s) in the overthrusting plate dipping north along the southern and central Hikurangi margin (model Y-200–120 km). To first-order, this gradual deepening of crustal material in the overthrusting plate appears consistent with surface geology, with the rocks exposed at the surface gradually younging or progressing up-section along the coast from south-to-north (Heron et al., 2015). In addition to these gradual changes in upper-plate wavespeeds, strike-parallel slices taken further landward reveal three abrupt discontinuities in the seismic velocity structure of the overthrusting plate (red arrows on Figures 10e and 10f). These are located in Cook Strait, north of Gisborne and across the northern tip of Raukumara Peninsula. The Cook Strait transition is marked by a near-vertical boundary in the 4.5 and 5.0 km/s isovelocity surfaces, and the thickness of surficial low velocity material (V_P 1.8–4.0 km/s) in Cook Strait increasing by up-to ∼4 km relative to the lower North Island (Figures 10e and 10f). The Gisborne boundary is marked by an abrupt ∼5 km northward increase in the depth of isovelocity surfaces and the

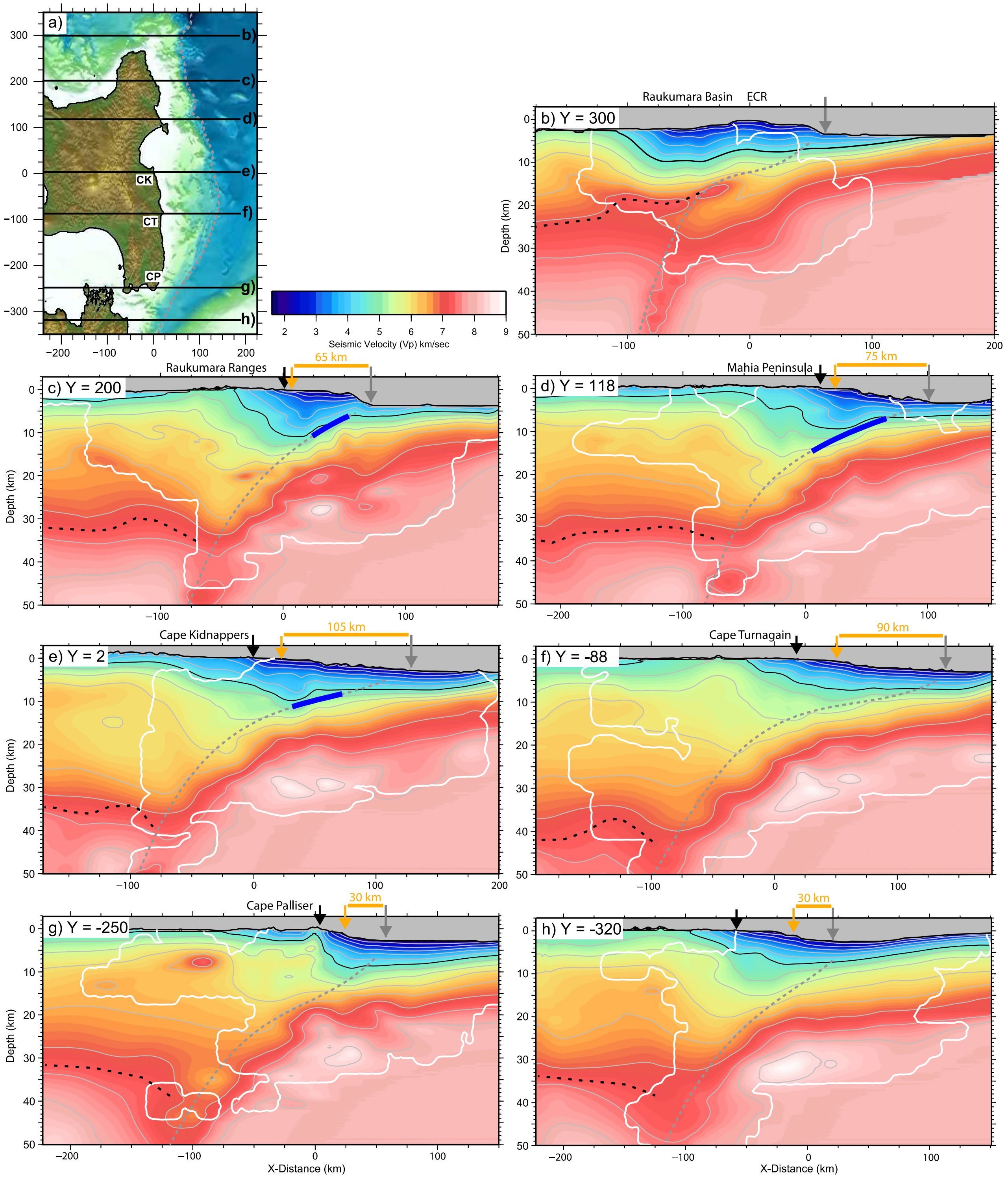

Figure 9. **Dip slices through the final P-wave velocity model of the Hikurangi margin.** (a) Map of the model domain showing the location of X-slices. (b)–(f) P-wave seismic velocity. White line shows the region of checkerboard recovery, indicating where the model is well-constrained. The top of the subducting Hikurangi Plateau is dashed in gray (Williams et al., 2013). Thick blue line shows where shallow cumulative slow-slip (2002–2014) exceeds 200 mm (Wallace, 2020; Wallace, Beavan, et al., 2012). The black line shows the 4.5 km/s iso-velocity contour, which approximates the updip extent of the crustal backstop. The updip extent of the crustal backstop is marked by the orange arrow, with the black and gray arrows marking the coastline and deformation front respectively. The orange bar (labeled) highlights strong along-strike variability in the proximity of the crustal backstop to the deformation front. Dotted black line approximates the overriding plate Moho. Annotation: CK = Cape Kidnappers, CT = Cape Turnagain; CP = Cape Palliser.

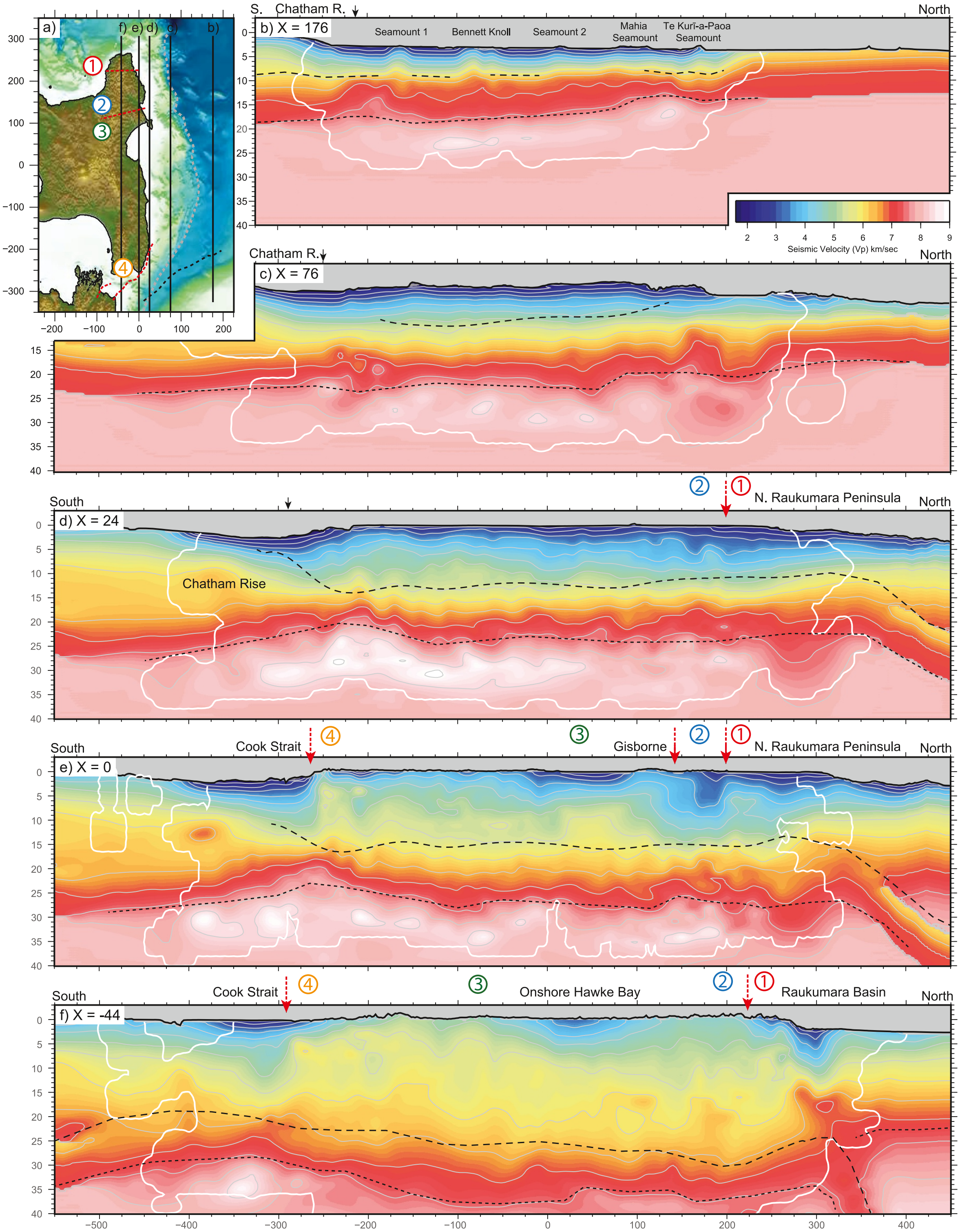

Figure 10. Strike slices through the final P-wave velocity model of the Hikurangi margin. (a) Map of the model domain showing the location of strike-slices. (b)–(f) P-wave seismic velocity. White line shows the region of checkerboard recovery, indicating where the model is well-constrained. The top of the subducting Hikurangi Plateau is dashed in gray (Williams et al., 2013), with our interpreted position for the Moho of the Hikurangi Plateau dotted in black. Note the south-to-north reduction in the crustal thickness of the Hikurangi Plateau. Red arrows (labeled) mark abrupt along-strike transitions in overthrusting plate structure. Black arrows mark the toe of the Chatham Rise beneath Pegasus Basin.

thickness of material overlying the subduction interface with $V_P \geq 5.0$ km/s reducing from 8 ± 1 to 1 ± 1 km (Figure 10e). This transition marks the southern boundary of the low-velocity wedge resolved in the dip-parallel slice across Raukumara Peninsula (Figure 9c). The northern tip of Raukumara Peninsula is marked by an increase in upper-plate wavespeeds, with isovelocity contours abruptly shallowing by ∼4 km from south-to-north (Figure 10e).

North of Raukumara Peninsula, Raukumara Basin is marked by the accumulation of up-to 7.5 km of low-velocity ($V_P \leq 4.0$ km/s) sediments, underlain by thin crust, which at ∼7 km in thickness is likely oceanic in nature (Figures 9b and 10f). Where our model is well determined, we interpret the Moho beneath Raukumara Basin (dashed black line) based on a smoothed representation of the steep velocity gradients that occur between 7–8 km/s. Although the smoothness of our velocity model makes Moho interpretations uncertain, the suggested Moho depth of ∼17–19 km is consistent with the results of prior modeling of onshore-offshore and OBS data (Bassett et al., 2010; Scherwath et al., 2010; Sutherland et al., 2009). This reduction in forearc Moho depth marks a transition from ocean-continent to ocean-ocean subduction, and the trenchward migration of the locus of forearc uplift from the Raukumara Ranges to the East Cape Ridge has been linked with the locus of lower-crustal underplating migrating eastwards in response to the thinner crust and more easterly location of the subducting slabs intersection with the forearc Moho (Bassett et al., 2010; Scherwath et al., 2010; Sutherland et al., 2009).

Seaward of the deformation front (Figure 10b), our model shows 5 seamounts on the incoming plate and reveals north-south variability in the crustal thickness of the Hikurangi Plateau. Following Bassett et al. (2023), we take 5.5 km/s to mark the top of the Hikurangi Plateau crust and interpret the Moho (as above) from the steep velocity gradients between 7–8 km/s. Where the Plateau is well constrained (Figure 10b), these criteria yield a crustal thickness that reduces from ∼10 to 11 km across the southern portion of the Plateau to ∼7–8 km further north. This difference in crustal thickness has been shown to extend farther east on the Plateau (Bassett et al., 2023). It also appears to persist along transects taken landward of the deformation front (e.g., Figure 10c), although our resolution and ability to detect changes in crustal thickness is limited given that we are only inverting first-arrivals.

Differences in crustal thickness appear associated with wavespeed variability in the underlying mantle. Seismic velocities beneath the region of thicker crust are, on average, 0.2–0.4 km/s faster than wavespeeds observed in the adjacent region of thinner crust and exceed 8.5 km/s beneath the southern portion of the Plateau (Figure 10d). These wavespeeds are similar to those previously resolved from controlled-source seismic studies in south Hikurangi (Bassett et al., 2022a, 2023; Herath et al., 2020; Stern et al., 2020) and over a greater depth range from earthquake tomography (Eberhart-Phillips et al., 2022). We are, however, mindful that checkerboard tests and Monte-Carlo analysis suggest uncertainties in wavespeeds in this region are ∼0.15–0.2 km/s, with the long offsets of our first arrivals insufficient to overcome trade-offs between crustal wavespeeds, crustal thickness and wavespeeds in the underlying mantle of the Hikurangi Plateau. South-to-north variability in mantle velocities may reflect differences in crustal thickness and curvature impacting the hydration and stress-state of the mantle or, alternatively, differences in the preservation or distribution of anisotropic fabrics that have been linked with high wavespeeds in south Hikurangi (Stern et al., 2020).

5. Discussion

5.1. Margin Structure From Spatial Variability in Wavespeeds

Seismic reflection data reveal a contrast in lower-crustal reflectivity between the inner and outer-portions of the forearc along the southern and central Hikurangi margin. The inner-portion is highly reflective and capped by a laterally continuous mid-crustal reflector. The outer-portion can be distinguished by a notable reduction in lower crustal reflectivity. The highly reflective unit has previously been interpreted as Cretaceous (110–100 Ma) Pahaoa Group rocks of the Torlesse Composite Terrane that constitutes geological basement in eastern North Island (Barker et al., 2009; Moore & Speden, 1979; Mountjoy & Barnes, 2011). This interpretation is supported by the regional interpretation of seismic reflection data sets that show the mid-crustal reflector that caps this unit shallowing toward the southeast (Bassett, Arnulf, Henrys, et al., 2022), where Pahaoa Group rocks outcrop in the coastal foothills of Wairarapa (Mortimer, 2004; Heron et al., 2015).

Figure 11 shows four seismic reflection profiles acquired in 2017 during the SHIRE experiment (Gase et al., 2022). The seismic reflection data have had a 3,000 ms Automatic Gain Control applied to highlight the distribution of the reflective unit and is overlain by velocity contours extracted from our 3D model and converted

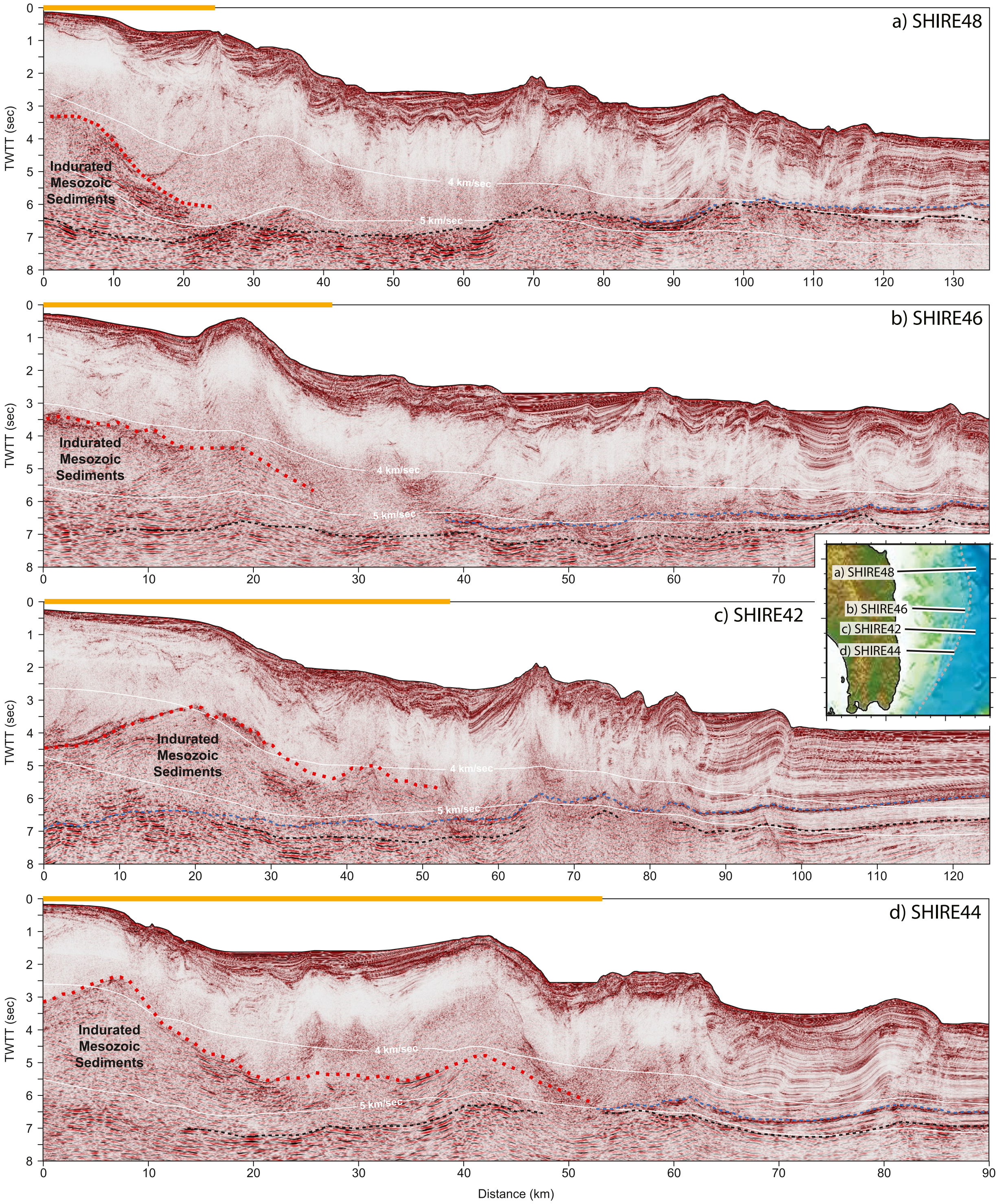

Figure 11. MCS constraints on backstop structure. Seismic reflection data illustrating MCS constraints on the distribution of Indurated Mesozoic sediments along (a) SHIRE48, (b) SHIRE46, (c) SHIRE42 and (d) SHIRE44 (Gase et al., 2022). Dashed red line shows the top of lower crustal high-reflectivity, which has previously been interpreted as Torlesse Basement (Bassett, Arnulf, Henrys, et al., 2022; Gase et al., 2022; Mountjoy & Barnes, 2011). White contours show the 4 and 5 km/s iso-velocity contours from our 3-D seismic velocity model converted to two-way-time. Although variable horizontally and in depth, the top of the Torlesse Basement typically corresponds to a wavespeed between 4.25 and 4.5 km/s. Dashed blue and black lines mark Sequence Y, and the top of the volcaniclastic sequence HKB of the Hikurangi Plateau, respectively, with the solid orange line illustrating the offshore extent of where the Torlesse basement overlies the subduction interface. Inset shows profile locations. The same sections with a simplified processing sequence are shown in Supplementary information (Figure S6 in Supporting Information S1).

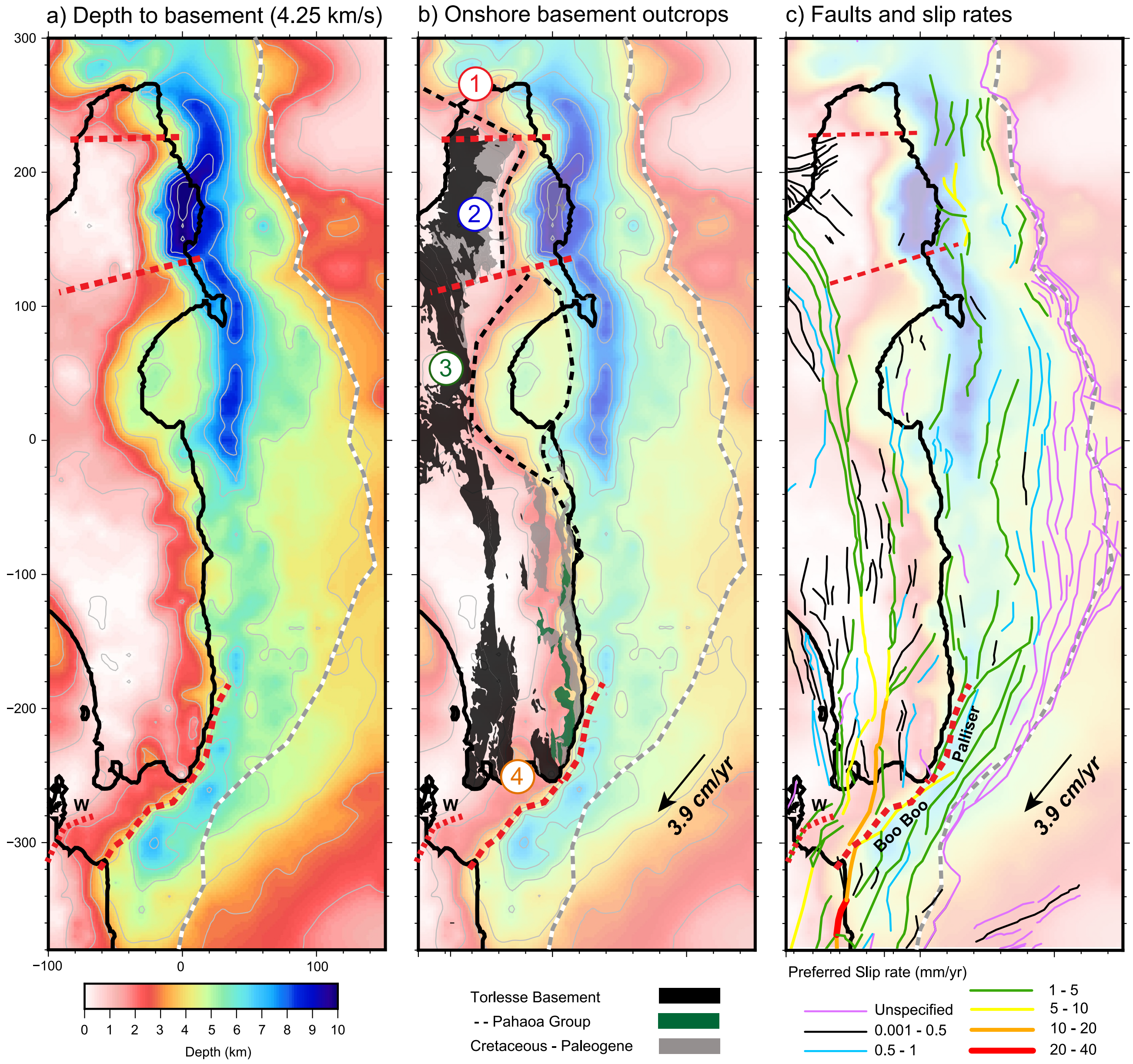

Figure 12. Depth to basement. (a) Map showing depth to the 4.25 km iso-velocity contour. Dashed gray line marks the deformation front. (b) As in (a) but overlying the surface distribution of Torlesse Basement and the Cretaceous-Paleogene cover sequence (Heron, 2014). Note the strong correlation between the predicted and observed surficial distribution of basement rocks. We suggest this correlation indicates that, to first-order, spatial variability in upper-plate wavespeeds primarily reflect the geological architecture of the overthrusting plate and the spatial distribution of terranes within it. Dashed red lines illustrate the map-view geometry of the sharp transitions in upper-plate wave speed identified from margin-normal cross-sections (Figure 10e). The numbered segments separated by these boundaries are interpreted in Section 5.2. Dotted red line (labeled W) marks a transition in crustal structure interpreted near the Wairau Fault. Dashed black lines approximate the strike of depth to basement contours. (c) As in (a) but overlying the Community Fault Model (Seebeck et al., 2024). Faults are colored according to slip-rate. The Cook Strait transition in crustal architecture may play a role in transferring strain accommodation from the subduction interface onto strike-slip faults in the upper-plate.

to two-way travel time. This comparison shows the reflective unit to be characterized by wavespeeds ≥4.25 ± 0.2 km/s at shallow depth beneath the inner wedge and slightly higher wavespeeds of ≥4.5 ± 0.2 km/s further offshore and at greater depth.

We use these wavespeed thresholds to identify the subsurface distribution (≥4.25 ± 0.2 km/s) and offshore extent (≥4.5 ± 0.2 km/s) of geological basement, respectively. The former is illustrated in Figure 12a, which shows depth to the 4.25 km/s isovelocity surface. Overlaying the surface distribution of Torlesse Basement (Figure 12b) reveals a good agreement between the predicted and observed distribution of geological basement. This correlation is consistent with prior associations between regions of high or moderate crustal reflectivity and Mesozoic indurated sediments (Mountjoy & Barnes, 2011). Moreover, it is an important observation as it suggests that to first order, wavespeed variability in the overthrusting plate is significantly influenced by geological architecture and the degree of induration of rocks within the overthrusting plate.

Figure 12 also provides a map view representation of along-strike changes in overthrusting-plate structure and seismic velocities that are identified in Figures 9 and 10. These changes (red dash in Figure 12a) are located across northern Raukumara Peninsula, near Gisborne and within Cook Strait, and bound four structural domains of the Hikurangi margin. In segment 1 (Raukumara), the depth to basement contours (dashed black line in Figure 12a) strike northwest in northern Raukumara Peninsula and Raukumara Basin. Seismic reflection data from Raukumara Basin tied to onshore exposures suggests that undeformed Cretaceous strata onlap this dipping surface of basement rock, which overlies an older thrust fault that is possibly the Mesozoic Gondwana margin (Sutherland et al., 2009). Segment 2 (Gisborne) strikes NNE and has a thick (>8 km) unit of deformed sediment adjacent to it, including deformed Cenozoic sediment. Segment 3 (Hawke Bay-Manawatu) strikes similarly to Segment 2, but exhibits a complex bifurcating geometry and variations in sediment thickness within Hawke Bay. Segment 4 (Palliser) strikes ENE and comes into close proximity (30 km) to the subduction thrust, that is, the wedge is narrowest in this region.

5.2. Origins of Along-Strike Segmentation of Crustal Architecture

To investigate the geological interpretation of discontinuities in forearc wavespeeds, Figure 13 shows a sequence of panels illustrating the tectonic evolution of the Hikurangi margin since the Early Oligocene, modified from the GPlates reconstruction of Seebeck et al. (2023).

Island arc thoeleiites of Eocene age recovered from the eastern flank of Tonga Ridge show west dipping subduction of the Pacific Plate initiated north of New Zealand along the northern Tonga arc at circa 52–48 Ma (Crawford et al., 2003; Meffre et al., 2012). The Tonga-Kermadec trench progressively lengthened southward and back-arc spreading centers formed. The oldest subduction-related lavas on Norfolk and Three Kings Ridge suggest that subduction occurred north of Northland at 36–26 Ma (Herzer et al., 2011; Mortimer et al., 2007; Orr et al., 2020; Sutherland et al., 2020). Emplacement of allochthons in Reinga Basin at 34–28 Ma and in Northland at 26–23 Ma, followed by arc volcanism after 23 Ma in Northland suggest subduction initiation was propagating east toward Raukumara Peninsula, but the precise geometry remains uncertain (Figure 13a).

Allochthons were emplaced westwards into Raukumara Basin and onto Raukumara Peninsula at 23–20 Ma (Sutherland et al., 2009). This event was possibility associated with the subduction trench jumping to a new position east of Raukumara Basin, resulting in the accretion of Raukumara Plain which formed from the captured piece of oceanic crust. At this time, Hikurangi subduction became established, possibly exploiting inherited faults that formed during Cretaceous collision of the Hikurangi Plateau with the continental margin (Figure 13b).

Trench rollback continued through the Miocene (Figures 13b and 13c) and was accompanied by widespread vertical-axis clockwise rotation of crustal blocks in eastern North Island. Paleomagnetic declination anomalies reveal clockwise rotations south of Gisborne and Māhia Peninsula (Segment 3) with the Wairoa Domain rotated clockwise up to 60–90° (Nicol et al., 2007; Thornley, 1996; Walcott, 1989). These large Cenozoic rotations in Segment 3 contrast with only small Cenozoic rotations in segments 1 and 2. We posit that large rotations south of segment 2 are related to southward propagation of the plate boundary during the Miocene as it linked via several crustal faults to the Alpine Fault system.

In the Miocene (Figure 13d), a throughgoing plate boundary formed as the main structure delineating the edge of Segment 4, The Boo-Boo-Palliser Fault System (Figure 13c), linked with the Alpine-Wairau fault (Seebeck et al., 2023). The Boo-Boo-Palliser Fault System was and still is aligned parallel to the plate motion vector and has likely accommodated substantial strike-slip displacement. The Wairau Fault accommodated ∼140 km of right lateral displacements during the Miocene and marks the northern boundary of the Marlborough domain, which contains blocks that experienced extensive (>50°) clockwise vertical axis rotations relative to the lower North Island since the Middle Miocene (Little & Roberts, 1997; Mortimer, 2004; Rowan & Roberts, 2008; Walcott et al., 1981). We follow previous authors in attributing north-to-south reductions in upper-plate wavespeeds and

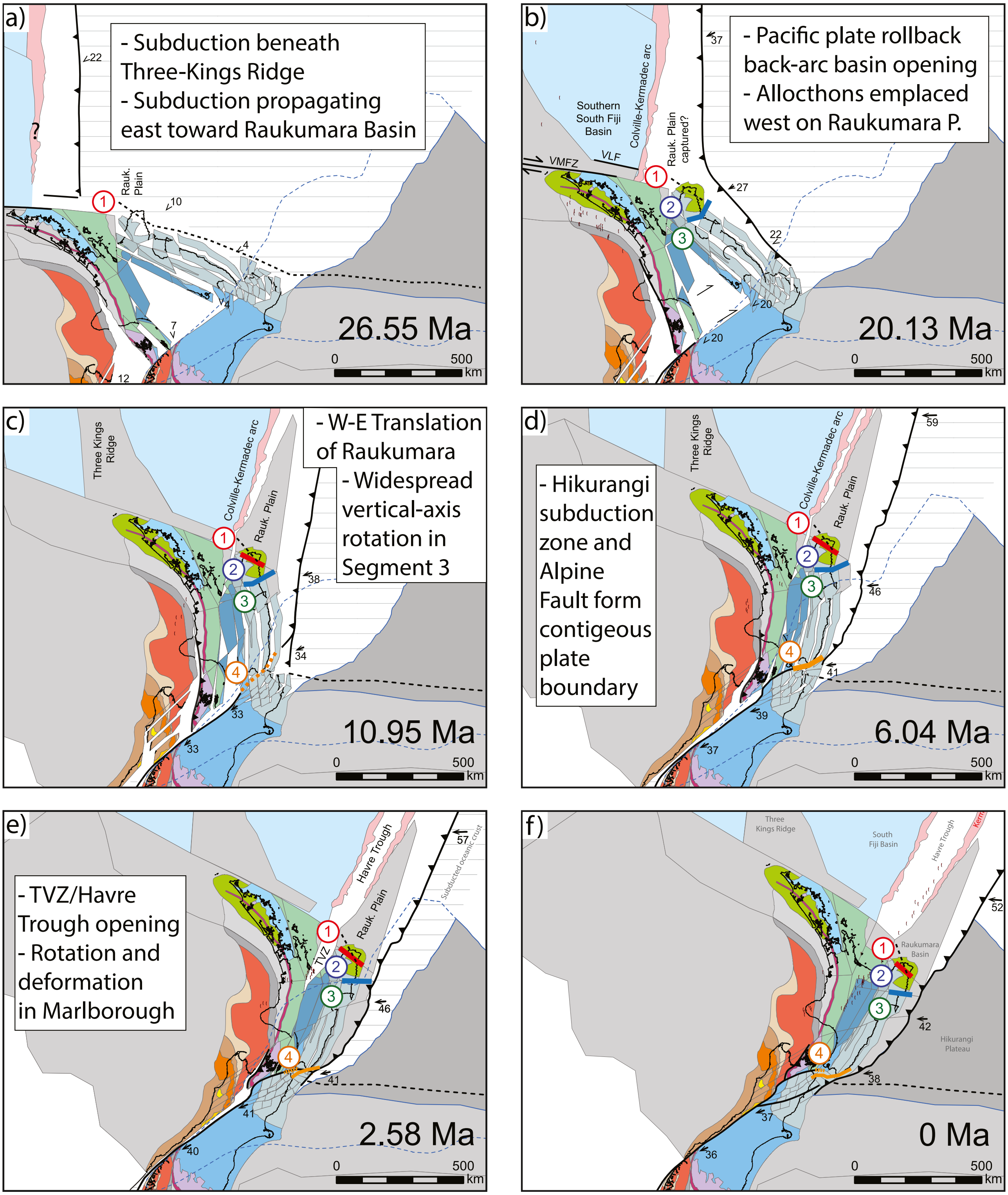

Figure 13. Tectonic evolution of the Hikurangi margin. (a)–(f) Panels showing the configuration of crustal blocks at different stages of the Hikurangi margin's tectonic evolution, modified from the GPlates reconstruction of Seebeck et al. (2023). Red, Blue and Orange bars mark the location of transitions in upper-plate wavespeeds resolved by our 3D seismic velocity model with numbers indicating margin segments. Dashed black and blue lines approximate the edge of the Cretaceous Gondwana margin and the edge of the Hikurangi Plateau (Reyners et al., 2011), respectively.

residual gravity anomalies in the Marlborough domain to differences in deformation, fracturing and fluid-content in the overthrusting plate (Henrys et al., 2020).

Progressive displacement and rotations at the plate boundary and the easterly migration of faulting across the Marlborough Fault System has mis-aligned the Boo-Boo-Palliser Fault System with the northern boundary of the Marlborough domain (offshore continuation of Wairau Fault). Now the Hope Fault links with the Boo-Boo-Palliser Fault System and this is the primary active linkage between the Alpine Fault and Hikurangi subduction thrust (Figures 13e–13f) (Barnes & deLepinay, 1997; Barnes et al., 2008; Langridge et al., 2016; Pondard & Barnes, 2010; Seebeck et al., 2024; Wallace, Barnes, et al., 2012).

Geological data suggest the Boo Boo fault is highly active and slips at ~10 mm/yr (Barnes et al., 2008; Litchfield et al., 2014; Pondard & Barnes, 2010; Seebeck et al., 2024), however, this may be even higher with new kinematic models constrained by plate motions requiring 23 mm/yr of dextral deformation to be accommodated between the South Wairarapa coast and Pacific Plate (Hirschberg & Sutherland, 2022). The geometrical continuity of the Palliser, Boo Boo, Needles and Kekerengu faults (Barnes et al., 2008; Hirschberg & Sutherland, 2022; Litchfield et al., 2014; Wallace, Barnes, et al., 2012), may make these faults likely candidates for accommodating a high proportion of this motion. Within Cook Strait and offshore Wairarapa, the Boo Boo and Palliser faults appear to have localized along the same inherited boundary in crustal structure (Figure 12c). This sharp boundary in crustal structure may play a role in focusing strain onto this sequence of faults and its combined length of ~180 km may translate to an earthquake with magnitude >8, if these faults are capable of rupturing together.

Overall, our interpretation implies a tectonic origin for along-strike transitions in seismic wavespeeds. The NW-SE orientation of depth to basement contours in Segment 1 (Figure 12a) is inherited from the Cretaceous. We also infer that Segment 2 geometry is inherited from the Cretaceous, but Cenozoic crustal underplating has exaggerated the height of the Raukumara ranges, thickened and deformed the sedimentary sequence, and tilted it eastward on the flanks of the ranges (Bassett et al., 2010). In segments 1 and 2, deformation accompanying allochthon emplacement (van de Lagemaat et al., 2022) and the prevalence of upper-plate extension may have contributed to preservation of such low seismic velocities. The structural contrast between segments 2 and 3 reflects major differences in Neogene deformation as the plate boundary propagated southward, with Segment 3 undergoing substantial deformation and clockwise rotation. We follow previous studies in associating crustal boundaries within Cook Strait and north-south differences in elastic properties with the structures and deformation that have linked the Hikurangi subduction zone with the Alpine Fault. Collectively, these interpretations support the notion described in Section 5.1 that wavespeed variability predominantly reflects the tectonic evolution and spatial distribution of geological domains in the overthrusting plate.

5.3. Backstop Geometry and Relationships With Shallow Megathrust Slip Behavior

The rigidity of materials overlying the subduction interface and the position of the crustal backstop have been suggested to play a key role in modulating shallow megathrust slip behavior (Bilek & Lay, 1999; Byrne et al., 1993; Nakanishi et al., 2002; Sallarès & Ranero, 2019; Ulrich et al., 2022). To obtain regional 3-D constraints on the updip extent of the Torlesse backstop, we have used the wavespeed threshold for the highly reflective lower-crust near the toe of the margin ($V_P \geq 4.5$ km/s–Figure 11) to estimate the thickness of Torlesse material overlying the subduction interface (Figure 14). To account for vertical smearing in wavespeeds and iso-velocity contours becoming subparallel with the downgoing plate as they approach the megathrust, the updip extent of the backstop (orange line in Figure 14) is interpreted where 2 km of crustal material overlies the subduction interface.

This calculation reveals substantial along-strike variability in the proximity of the crustal backstop to the deformation front and is consistent with along-strike differences in the width of the outer-forearc interpreted from margin normal cross-sections (Figure 9). Along the southern Hikurangi margin, the backstop is parallel and close-to the deformation front, only increasing gradually from a location just 25 km from the deformation front offshore Cape Palliser to 35 km from the deformation front south of Cape Turnagain (Figure 14a). North of Cape Turnagain, the backstop appears to retreat down-dip by ~70 km to a position located ~100 km from the deformation near Aramoana. North of Aramoana, the backstop is approximately parallel to the coastline striking ~31°, with slight obliquity with respect to the trench (~21°) gradually reducing the distance to the deformation front from ~100 km at Aramoana to 80 km at Māhia and 60 km at Tolaga Bay (Figure 14a).

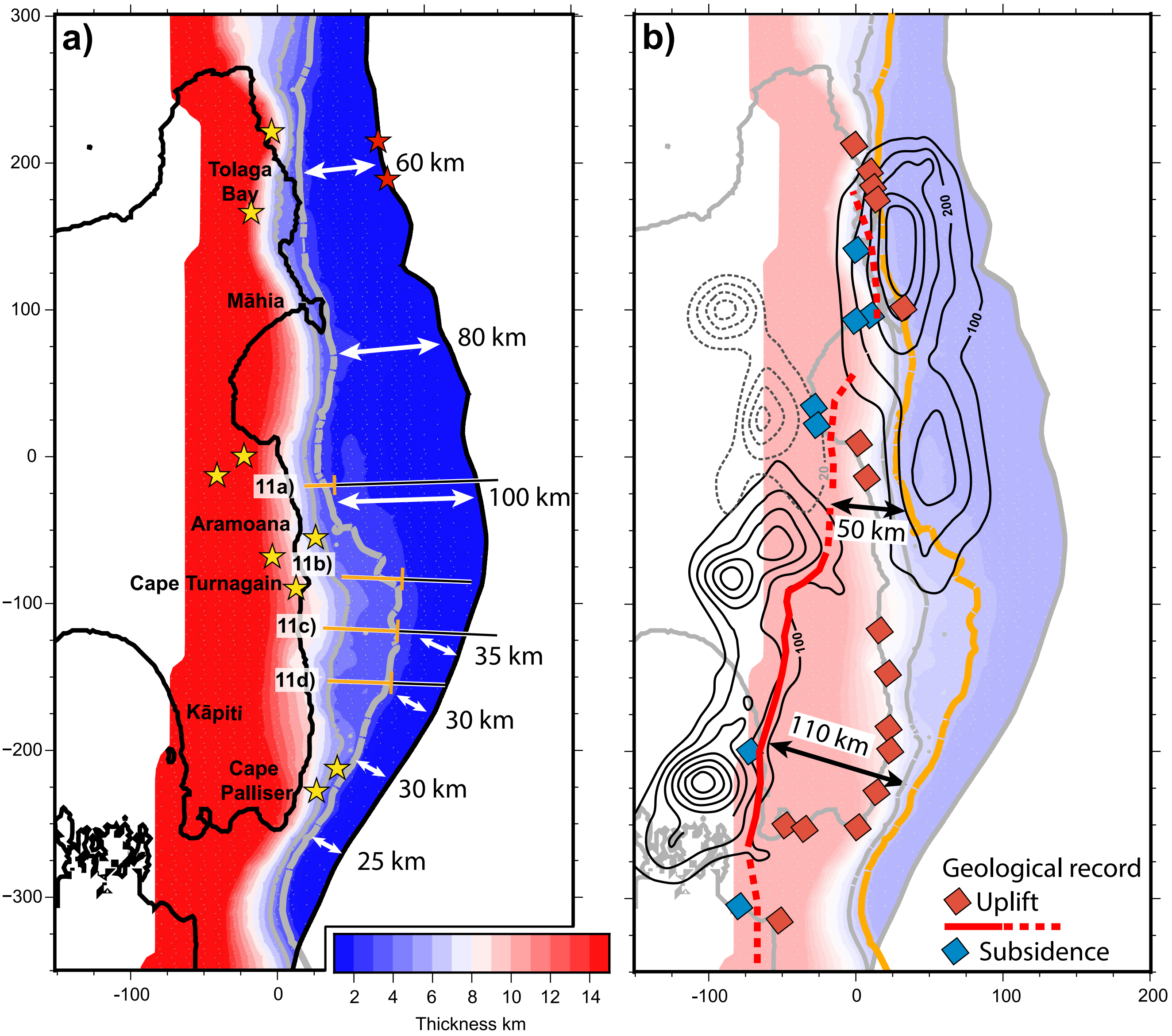

Figure 14. **Backstop geometry.** (a) Backstop geometry along the Hikurangi margin. Color and contours show the thickness of Torlesse rocks ($V_P \geq 4.5$ km/s) overlying the subduction interface and the updip extent of the Torlesse backstop. Arrows (labeled) highlight strong along-strike variability in the updip extent of the backstop. Yellow stars show locations of historic subduction interface events (Downes, 2006; Webb & Anderson, 1998). Red stars mark tsunami earthquakes (Bell et al., 2014; Downes et al., 2000). (b) Relationship between the backstop geometry (Orange line) and cumulative distribution of shallow slow-slip (black contours) (Wallace, 2020). Solid red line marks the downdip limit of frictional locking in current plate coupling models (Wallace, Beavan, et al., 2012). Through the central and northern margin, this limit is estimated from the updip extent of deep SSEs and the distribution of uplift (red diamonds) and subsidence (blue diamonds) in the geological record of past earthquakes (Clark et al., 2019).

Prior constraints on the geometry of the backstop had focussed on the distribution of high lower-crustal reflectivity within the inner-forearc and in particular, the relationship with onshore geology (Bassett, Arnulf, Henrys, et al., 2022). The key difference from these prior constraints is that our calculation shows the backstop maintaining a position near the deformation front along the southern Hikurangi margin. This calculation is consistent with the margin-normal extent of high-lower-crustal reflectivity (solid orange lines in Figures 11 and 14a) in new high-quality deep-penetration SHIRE MCS data sets (Gase et al., 2022).

The updip extent of co-seismic slip is a key control on tsunami excitation and a range of studies have linked depth-dependent earthquake rupture behavior with margin-normal transitions in the rigidity of materials overlying the megathrust (Bilek & Lay, 1999; Byrne et al., 1988; Kopp & Kukowski, 2003; Lay et al., 2012; Sallarès et al., 2021; Sallarès & Ranero, 2019). In SW Japan, a directly analogous 3-D seismic velocity model of Nankai Trough showed the crustal backstop to be well correlated with the updip extent of strong interseismic coupling (Nishimura et al., 2018) and the shallow transition from seismic (unstable) to aseismic (stable/conditionally stable) megathrust slip (Bassett, Arnulf, Kodaira, et al., 2022). At Hikurangi, the absence of seafloor geodetic data in current plate locking models means that the offshore extent of frictional locking is not well constrained (Wallace, Barnes, et al., 2012). Shallow slow-slip along the central and north Hikurangi margin occurs predominantly updip of the crustal backstop and the southern limit of shallow slow-slip occurs near where the crustal backstop extends ~70 km further updip causing the outer-forearc to narrow from ~100 to ~35 km in width (Figure 14b). This may suggest the relationships observed in SW Japan between the position of the backstop and the downdip limit of shallow conditional stability may also be applicable at Hikurangi. This link may reflect differences in induration or frictional properties (Moore & Speden, 1984), the strength and stress-state of the wedge and/or the mechanics by which it accumulates and releases elastic strain (Sallarès & Ranero, 2019). Differences in overthrusting plate density will also translate to variations in normal stress at the subduction interface, and although significantly smaller than margin-normal stress increases associated with overburden thickness, the influence on effective normal stress may be greater if differences in induration impact structural permeability and the ability of the wedge to maintain or relieve excess fluid pressure (Reyners & Eberhart-Phillips, 2009).

If the relationships observed in SW Japan *are* applicable at Hikurangi, the implication is that there is a higher likelihood of shallow or trench-breaching seismic rupture along the southern Hikurangi margin, where the crustal backstop is located within 25–35 km of the deformation front (Hu & Wang, 2008) (Figure 14a). This distance is comparable to the ~30 km width of the outer-wedge where the 2011 M9 Tohoku-oki earthquake maintained large co-seismic slip amplitudes to the NE Japan trench (Miura et al., 2005).

5.4. Implications for the Dimensions and Slip Behavior of the Seismogenic Zone

Figure 15 illustrates how crustal-scale architecture and potentially upper-plate stress state impact the down-dip width of frictional locking. In south Hikurangi, the crustal backstop is located 25–35 km from the deformation front and strong-interseismic coupling beneath Kapiti extends to ~35–40 km depth (Wallace, Barnes, et al., 2012). If, as in SW Japan, strong interseismic coupling extends as far updip as the crustal backstop, this would suggest frictional locking in south Hikurangi occurs over a down-dip width of ~100 km (Figures 14b and 15e). North of Cape Turnagain, a shallowing of deep slow-slip events (<20–25 km) has been linked with the upper-plate stress state flipping from compression to extension and a reduction in the depth of the brittle-ductile transition (Fagereng & Ellis, 2009; Wallace, Fagereng, & Ellis, 2012). At the same location along-strike, the backstop migrates landward by ~70 km, which collectively, may reduce the zone of frictional locking to as little ~50 km (Figures 14b and 15d). A narrow corridor of locking in this region has been postulated by Wallace (2020) and is consistent with observations of contractional strain (Dimitrova et al., 2016; Haines & Wallace, 2020) and the occurrence of large earthquakes in 1904, 1958 and 1993 (Yellow stars, Figure 14a).

Paleoseismic and paleotsunami evidence suggest that up to nine earthquakes may have involved some component of slip on the central Hikurangi megathrust in the last 7,000 years (Clark et al., 2019; Pizer et al., 2021, 2023). The updip extent of slip in these events is unknown and it is unclear whether the portion of megathrust between the crustal backstop and zones of coastal subsidence (blue diamonds in Figure 14b), in conjunction with slip on upper-plate faults, is sufficient to explain coastal deformation and tsunami observations (Clark et al., 2019; Delano et al., 2023; Pizer et al., 2023). Alternatively, it is possible some portion of the zone updip of the crustal backstop is capable of rupturing both seismically and in SSEs (Clark et al., 2019), which may be a consequence of incoming plate roughness and associated heterogeneity in the structure, lithology and frictional properties of the megathrust (Barnes et al., 2020; Gase et al., 2022; Skarbek et al., 2012). In this mixed-mode scenario, the ability of co-seismic slip to propagate updip of the backstop may be impacted by its pre-stress and the time that has elapsed since the last slow-slip event. Despite this uncertainty, we suggest abrupt changes in backstop geometry and the depth of the brittle-ductile transition (Fagereng & Ellis, 2009; Wallace, Fagereng, & Ellis, 2012), superimposed on the gradual steepening of the subducting slab (Williams et al., 2013), results in a significant south-to-north reduction in the down-dip width of frictional locking across Cape Turnagain. This interpretation is highly analogous to Nankai Trough where a similar pinching of the seismogenic zone between Shikoku (~120 km) and Kyushu (<60 km) appears to impact both the margin-normal extent and magnitude of megathrust earthquakes (Bassett, Arnulf, Kodaira, et al., 2022; Bassett et al., 2025).

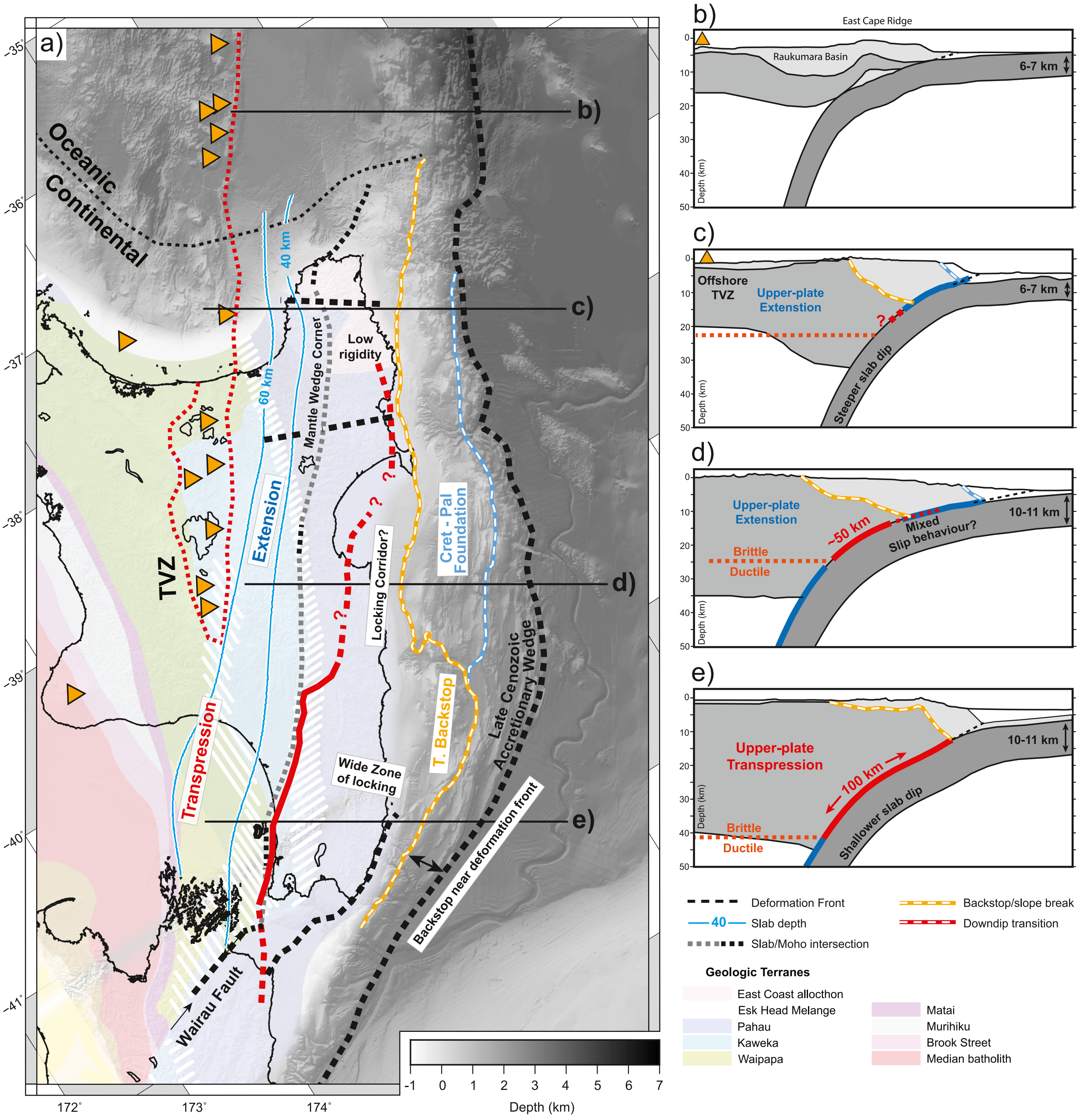

Figure 15. Margin architecture and dimensions of the seismogenic zone. (a) Map of the Hikurangi margin illustrating spatial variability in the distribution of recently accreted sediments, geological terranes and the mantle wedge overlying the megathrust. Dashed black lines onshore show the sharper, along strike-strike transitions in upper-plate properties related to the tectonic evolution of the Hikurangi margin. (b)–(e) Schematic cross-sections illustrating how this variability in upper-plate structure, in conjunction with changes in slab thickness and dip (Bassett et al., 2023; Williams et al., 2013), and upper-plate stress-state and depth to the brittle-ductile transition (Fagereng & Ellis, 2009; Wallace, Fagereng, & Ellis, 2012) impact the dimensions of the seismogenic zone.

The final implication is the impact of along-strike transitions in upper-plate structure on megathrust earthquakes, associated ground shaking and tsunami. In north Hikurangi, Kaneko et al. (2019) recognised that long-period (>10 s) ground motions associated with the 2016 M7.8 Kaikoura earthquake lasted for more than 450 s and postulated the presence of extremely low velocities in the overthrusting plate as a mechanism of generating the long duration ground motions. Our seismic velocity model resolves northward reductions in upper-plate wave-speeds at Cape Turnagain associated with the increasing width of the outer-forearc and more landward position of the crustal backstop (Figure 10b), and an abrupt reduction in upper-plate wavespeeds near Gisborne (Figures 10e and 12b). This latter transition is striking, marking the southern boundary of a wide region (∼120 km) in which extremely low wavespeeds (≤3.5 km/s to ∼7 km depth) are preserved in the overthrusting plate. These observations are consistent with the model and predictions of Kaneko et al. (2019) and demonstrate how heterogeneity in overthrusting plate wavespeeds resolved throughout our model may impact the duration of earthquake ground motions.

The low wavespeeds resolved north of Gisborne may also impact tsunamigenic trade-offs between slip to the trench, splay faulting and bulk yielding of the accretionary wedge (Ulrich et al., 2022). Dynamic rupture models show low rigidity in the overthrusting plate diminishes near-trench slip, but enhances off-fault plastic strain within the wedge (Ulrich et al., 2022). This latter effect can lead to tsunami up to a factor of two larger than scenarios in which slip extends to the trench and may have contributed to the generation of tsunami earthquakes offshore Gisborne and Tolaga Bay in 1947.

In south Hikurangi, our model resolves an abrupt southward reduction in upper-plate wavespeeds in Cook Strait and is consistent with earlier seismic velocity models (Henrys et al., 2020) and tectonic reconstructions associating this boundary with the northern boundary of the Marlborough domain (Little & Roberts, 1997; Seebeck et al., 2023; Walcott, 1978). South of this boundary, GPS and InSAR data recorded a pulse of postseismic afterslip following the 2016 M7.8 Kaikoura earthquake, reflecting velocity strengthening behavior on the subduction interface beneath Marlborough and Cook Strait (Wallace et al., 2018). Geological data and kinematic models also reveal a greater proportion of relative plate motion being accommodated via upper-plate structures in Cook Strait (e.g., the Boo Boo Fault) (Barnes & deLepinay, 1997; Barnes et al., 1998; Hirschberg & Sutherland, 2022; Litchfield et al., 2014; Wallace, Barnes, et al., 2012). Both factors will reduce the slip-deficit rate on the subduction interface beneath Cook Strait and Marlborough, and raise the possibility of steep spatial gradients in the strength or loading rate of the megathrust.

Numerical models of earthquake cycles show that interseismic stress increases are amplified near asperities where changes in fault strength occur over a shorter wavelength than the extent of stress shadowing (Hetland & Simons, 2010; Kanamori, 1981; Kaneko et al., 2010). Dynamic rupture simulations also show that dynamic rupture fronts decelerate as they penetrate into unloaded, velocity-strengthening, or compliant (less rigid) regions, which may ultimately arrest co-seismic ruptures (Tinti et al., 2005). It is possible, therefore, that differences in loading rate, fault strength and the elastic properties of the overthrusting plate between the lower North Island and Cook Strait may impact the dimensions and amplitudes of co-seismic slip in future earthquakes. This effect was most recently demonstrated during the 2011 M9 Tohoku-oki earthquake, where a similar inherited tectonic boundary known as the Median Tectonic Line (MTL) appeared to play a key role in separating regions of large co-seismic slip to the north from the region of post-seismic afterslip to the south (Bassett, Sandwell, et al., 2016; Sun et al., 2014). There, it was proposed that interseismic creep south of the MTL and the sharp contrast in frictional properties may have contributed to both the small rupture area and large amplitude of co-seismic slip in the Tohoku earthquake. We suggest the structural similarities between Cook Strait and the MTL in NE Japan are sufficient that understanding the nature of this boundary in greater detail and its potential impact on the dimensions and slip-amplitude of future earthquakes is an important topic of future research. It is similarly important to note that despite the reduction in the down-dip width of the seismogenic zone, our model does not resolve the presence of a structural boundary between the southern and central Hikurangi margin that may limit the along-strike extent of earthquakes.

6. Conclusions

We integrate four decades of onshore-offshore, OBS and onshore seismic data to construct a high-resolution, 3-D seismic velocity model of the Hikurangi subduction zone. From this, we draw the conclusions below.

1. Integrating controlled-source seismic data sets recorded onshore and offshore is a powerful method for obtaining high-resolution, regional 3-D constraints on the architecture of entire subduction zones. Incorporating and preserving shallow seismic velocity constraints from seismic reflection data sets is effective in reducing uncertainties and trade-offs in seismic wavespeeds, if dense 3-D distributions of short-offset raypaths from OBS surveys are not available.
2. The crust of the subducting Hikurangi Plateau reduces in thickness from 10 to 11 km along the southern Hikurangi margin to 6–7 km along the northern Hikurangi margin. Wavespeeds in the subducting mantle are

systematically higher (up-to 8.5 km/s) beneath the southern region of thicker crust. This difference may reflect anisotropy or the impact of crustal thickness and curvature on the hydration and stress-state of the mantle.

3. In the overthrusting plate, comparisons between the seismic velocity structure with onshore geology and subsurface structure from seismic reflection data sets reveal a strong agreement between the predicted and observed onshore distribution of geological basement (indurated Mesozoic sediment). This correlation indicates that to first order, wavespeed variability in the overthrusting plate is significantly influenced by the spatial distribution of geological domains, that is, differences in rock type.
4. Abrupt transitions in overthrusting plate structure are resolved in Cook Strait, near Gisborne and across the northern tip of Raukumara Peninsula. These can be associated with tectonic evolution of the Hikurangi margin (Seebeck et al., 2023) and show how tectonic inheritance and accumulated geological history since 25 Ma influences crustal structure, present kinematics and megathrust behavior.
5. The updip limit of the crustal backstop varies significantly along the Hikurangi margin. It is located just 25–35 km from the trench along southern Hikurangi margin, which may amplify tsunami hazard and the likelihood of trench-breaking rupture.
6. North of Cape Turnagain, the backstop retreats landward by ∼70 km and is located 80–100 km from the deformation front along the central Hikurangi margin. This landward retreat, in conjunction with a possible reduction in the depth of deep slow-slip and the brittle ductile transition, may reduce the down-dip width of frictional locking between the southern (∼100 km) and central Hikurangi margin by up-to 50%.
7. Extremely low- wavespeeds (3.5 km/s at ∼7 km depth offshore) are preserved north of Gisborne within a ∼120 km wide wedge extending 50 km onshore and up-to 12 km depth. Low velocities increase the duration of long-period shaking in large earthquakes (Kaneko et al., 2019) and may enhance the contribution of bulk yielding of the accretionary wedge to tsunami generation (Ulrich et al., 2022).
8. An abrupt transition in overthrusting plate structure in Cook Strait appears associated with a change in megathrust slip behavior and the diversion of relative plate motions from the megathrust onto strike-slip faults in the upper-plate. This inherited structure appears similar to the Median Tectonic Line that played a key role in modulating the distribution and amplitude of slip in the 2011 Tohoku-oki earthquake. Understanding these structures and their potential role in producing or limiting the dimensions of future earthquakes is an important topic of future research.

Conflict of Interest

The authors declare no conflicts of interest relevant to this study.

Data Availability Statement

Our seismic velocity model is available from Bassett (2024, https://zenodo.org/records/13381669). Seismic waveforms recorded by GeoNet seismometers are available from GNS Science (2024, https://www.geonet.org.nz/data/types/seismic_waveforms). Raw and processed marine multi-channel seismic (MCS) data used in this study are available through Bangs et al., 2017, https://www.marine-geo.org/tools/search/DataSets.php?data_set_uids=24459,24460,24461,24462. Ocean Bottom Seismograph data are available from GNS Science (2017, https://data.gns.cri.nz/metadata/srv/eng/catalog.search#/metadata/e3a620a4-d21e-41f8-8c5e-1fa1d7433279) and the JAMSTEC Seismic Survey Database (Barker, 2017, http://www.jamstec.go.jp/obsmcs_db/e/survey/data_area.html?cruise=TAN1710).

Acknowledgments

This study was supported by U.S National Science Foundation Grants: 1658010, 1657480 and 1615815, by the New Zealand Ministry of Business Innovation and Employment (MBIE) Endeavour Grants: Diagnosing peril posed by the Hikurangi subduction zone (C05X1605); and Ngā Ngaru Wakapuke–Building resilience to future earthquake sequences (contract number RTVU2306); by a Royal Society of New Zealand Marsden Fund Grant (MFP-GNS1902), and by public research funding from the MBIE Science Investment Fund to GNS Science. We thank the Captain and crew of the R/V *M.G. Langseth* (MGL1708) and R/V *Tangaroa* (TAN1710). We also thank MBIE and the Tangaroa Reference Group for its support in granting ship time on NIWA's Research Vessel *Tangaroa* during the TAN1710 voyage. Seismic processing and interpretation were conducted using GLOBE Claritas and Seisware. Figures were constructed using the Generic Mapping Tools (Wessel et al., 2019; Wessel & Smith, 1991). We thank Anne Trehu and an anonymous reviewer for detailed and constructive reviews that improved the manuscript.

References

Aniko Wirp, S., Gabriel, A.-A., Schmeller, M. H., Madden, E., van Zelst, I., Krenz, L., et al. (2021). 3D linked subduction, dynamic rupture, tsunami, and inundation modeling: Dynamic effects of supershear and tsunami earthquakes, hypocenter location, and shallow fault slip. *Frontiers in Earth Science*, *9*, 626844. https://doi.org/10.3389/feart.2021.626844

Arai, R., Kodaira, S., Henrys, S., Bangs, N., Obana, K., Fujie, G., et al. (2020). Three-Dimensional P wave velocity structure of the northern Hikurangi margin from the NZ3D experiment: Evidence for fault-bound anisotropy. *Journal of Geophysical Research: Solid Earth*, *125*(12), e2020JB020433. https://doi.org/10.1029/2020jb020433

Arai, R., Shiraishi, K., Nakamura, Y., Fujie, G., Miura, S., Kodaira, S., et al. (2024). Thick slab crust with rough basement weakens interplate coupling in the western Nankai Trough. *Earth Planets and Space*, *76*(1), 73. https://doi.org/10.1186/s40623-024-02025-4

Arnulf, A., Harding, A., Kent, G., & Wilcock, W. (2018). Structure, seismicity, and accretionary processes at the hot spot-influenced Axial Seamount on the Juan de Fuca Ridge. *Journal of Geophysical Research: Solid Earth*, *123*(6), 4618–4646. https://doi.org/10.1029/2017jb015131

Arnulf, A. F., Bassett, D., Harding, A. J., Kodaira, S., Nakanishi, A., & Moore, G. (2022). Upper-plate controls on subduction zone geometry, hydration and earthquake behaviour. *Nature Geoscience*, *15*(2), 143–148. https://doi.org/10.1038/s41561-021-00879-x

Bangs, N., Arnulf, A., van Avendonk, H., Saffer, D., Proctor, W., Okaya, D., et al. (2017). Project SHIRE: Seismogenesis at Hikurangi integrated research experiment [Dataset]. *Lamont Academic Seismic Portal*. https://doi.org/10.7284/907693

Bangs, N. L., Morgan, J. K., Bell, R. E., Han, S., Arai, R., Kodaira, S., et al. (2023). Slow slip along the Hikurangi margin linked to fluid-rich sediments trailing subducting seamounts. *Nature Geoscience*, *16*(6), 1–8. https://doi.org/10.1038/s41561-023-01186-3

Barker, D. H., Henrys, S., Caratori Tontini, F., Barnes, P. M., Bassett, D., Todd, E., & Wallace, L. (2018). Geophysical constraints on the relationship between seamount subduction, slow slip, and tremor at the north Hikurangi subduction zone, New Zealand. *Geophysical Research Letters*, *45*(23), 12804–12813. https://doi.org/10.1029/2018gl080259

Barker, D. H. N. (2017). TAN1710 – Deployment and recovery of Ocean Bottom seismometers during the sesimogenesis at Hikurangi integrated research experiment. *JAMSTEC Seismic Survey Database*. [Dataset] URL http://www.jamstec.go.jp/obsmcs_db/e/survey/data_area.html?cruise=TAN1710

Barker, D. H. N., Sutherland, R., Henrys, S., & Bannister, S. (2009). Geometry of the Hikurangi subduction thrust and upper plate, North Island, New Zealand. *Geochemistry, Geophysics, Geosystems*, *10*(2). https://doi.org/10.1029/2008gc002153

Barnes, P., Pondard, N., Lamarche, G., Mountjoy, J., Van Dissen, R., & Litchfield, N. (2008). It's our fault: Active faults and earthquake sources in Cook Strait: NIWA client report.

Barnes, P. M., & de Lepinay, B. M. (1997). Rates and mechanics of rapid frontal accretion along the very obliquely convergent southern Hikurangi margin, New Zealand. *Journal of Geophysical Research: Solid Earth*, *102*(B11), 24931–24952. https://doi.org/10.1029/97jb01384

Barnes, P. M., de Lepinay, B. M., Collot, J. Y., Delteil, J., & Audru, J. C. (1998). Strain partitioning in the transition area between oblique subduction and continental collision, Hikurangi margin, New Zealand. *Tectonics*, *17*(4), 534–557. https://doi.org/10.1029/98tc00974

Barnes, P. M., Lamarche, G., Bialas, J., Henrys, S., Pecher, I., Netzeband, G. L., et al. (2010). Tectonic and geological framework for gas hydrates and cold seeps on the Hikurangi subduction margin, New Zealand. *Marine Geology*, *272*(1), 26–48. https://doi.org/10.1016/j.margeo.2009.03.012

Barnes, P. M., Wallace, L. M., Saffer, D. M., Bell, R. E., Underwood, M. B., Fagereng, A., et al. (2020). Slow slip source characterized by lithological and geometric heterogeneity. *Science Advances*, *6*(13), eaay3314. https://doi.org/10.1126/sciadv.aay3314

Bassett, D. (2024). 3D P-Wave seismic velocity model for the Hikurangi subduction zone [Dataset]. *Zenodo*. https://doi.org/10.5281/zenodo.13381669

Bassett, D., Arnulf, A., Henrys, S., Barker, D., van Avendonk, H., Bangs, N., et al. (2022). Crustal structure of the Hikurangi margin from SHIRE seismic data and the relationship between forearc structure and shallow megathrust slip behavior. *Geophysical Research Letters*, *49*(2), e2021GL096960. https://doi.org/10.1029/2021gl096960

Bassett, D., Arnulf, A., Kodaira, S., Nakanishi, A., Harding, A., & Moore, G. (2022). Crustal structure of the Nankai subduction zone revealed by two decades of onshore-offshore and ocean-bottom seismic data: Implications for the dimensions and slip behavior of the seismogenic zone. *Journal of Geophysical Research: Solid Earth*, *127*(10), e2022JB024992. https://doi.org/10.1029/2022jb024992

Bassett, D., Fujie, G., Kodaira, S., Arai, R., Yamamoto, Y., Henrys, S., et al. (2023). Heterogeneous crustal structure of the Hikurangi Plateau revealed by SHIRE seismic data: Origin and implications for plate boundary tectonics. *Geophysical Research Letters*, *50*(22), e2023GL105674. https://doi.org/10.1029/2023gl105674

Bassett, D., Kopp, H., Sutherland, R., Henrys, S., Watts, A. B., Timm, C., et al. (2016). Crustal structure of the Kermadec arc from MANGO seismic refraction profiles. *Journal of Geophysical Research*, *121*(10), 7514–7546. https://doi.org/10.1002/2016jb013194

Bassett, D., Sandwell, D. T., Fialko, Y., & Watts, A. B. (2016). Upper-plate controls on co-seismic slip in the 2011 Magnitude 9.0 Tohoku-oki earthquake. *Nature*, *531*(7592), 92–96. https://doi.org/10.1038/nature16945

Bassett, D., Shillington, D. J., Wallace, L. M., & Elliott, J. L. (2025). Variation in slip behaviour along megathrusts controlled by multiple physical properties. *Nature Geoscience*, *18*(1), 20–31. https://doi.org/10.1038/s41561-024-01617-9

Bassett, D., Sutherland, R., & Henrys, S. (2014). Slow wavespeeds and fluid overpressure in a region of shallow geodetic locking and slow slip, Hikurangi subduction margin, New Zealand. *Earth and Planetary Science Letters*, *389*, 1–13. https://doi.org/10.1016/j.epsl.2013.12.021

Bassett, D., Sutherland, R., Henrys, S., Stern, T., Scherwath, M., Benson, A., et al. (2010). Three-dimensional velocity structure of the northern Hikurangi margin, Raukumara, New Zealand: Implications for the growth of continental crust by subduction erosion and tectonic underplating. *Geochemistry, Geophysics, Geosystems*, *11*(10). https://doi.org/10.1029/2010gc003137

Bell, R., Holden, C., Power, W., Wang, X., & Downes, G. (2014). Hikurangi margin tsunami earthquake generated by slow seismic rupture over a subducted seamount. *Earth and Planetary Science Letters*, *397*, 1–9. https://doi.org/10.1016/j.epsl.2014.04.005

Bell, R., Sutherland, R., Barker, D., Henrys, S., Bannister, S., Wallace, L., & Beavan, J. (2010). Seismic reflection character of the Hikurangi subduction interface, New Zealand, in the region of repeated Gisborne slow slip events. *Geophysical Journal International*, *180*(1), 34–48. https://doi.org/10.1111/j.1365-246x.2009.04401.x

Bilek, S. L., & Lay, T. (1999). Rigidity variations with depth along interplate megathrust faults in subduction zones. *Nature*, *400*(6743), 443–446. https://doi.org/10.1038/22739

Bland, K. J., Uruski, C. I., & Isaac, M. J. (2015). Pegasus Basin, eastern New Zealand: A stratigraphic record of subsidence and subduction, ancient and modern. *New Zealand Journal of Geology and Geophysics*, *58*(4), 319–343. https://doi.org/10.1080/00288306.2015.1076862

Byrne, D. E., Davis, D. M., & Sykes, L. R. (1988). Loci and maximum size of thrust earthquakes and the mechanics of the shallow region of subduction zones. *Tectonics*, *7*(4), 833–857. https://doi.org/10.1029/tc007i004p00833

Byrne, D. E., Wang, W. h., & Davis, D. M. (1993). Mechanical role of backstops in the growth of forearcs. *Tectonics*, *12*(1), 123–144.

Chadwick, M. P. (1997). *The 1991 Hikurangi margin seismic refraction experiment: A thesis submitted [to the] Victoria university of Wellington [in fulfilment of the requirements] for the degree of doctor of philosophy in geophysics*. Victoria University of Wellington.

Chesley, C., Naif, S., & Key, K. (2023). Characterizing the porosity structure and gas hydrate distribution at the southern Hikurangi Margin, New Zealand from offshore electromagnetic data. *Geophysical Journal International*, ggad243.

Chesley, C., Naif, S., Key, K., & Bassett, D. (2021). Fluid-rich subducting topography generates anomalous forearc porosity. *Nature*, *595*(7866), 255–260. https://doi.org/10.1038/s41586-021-03619-8

Chow, B., Kaneko, Y., Tape, C., Modrak, R., Mortimer, N., Bannister, S., & Townend, J. (2022). Strong upper-plate heterogeneity at the Hikurangi subduction margin (North Island, New Zealand) imaged by adjoint tomography. *Journal of Geophysical Research: Solid Earth*, *127*(1), e2021JB022865. https://doi.org/10.1029/2021jb022865

Clark, K., Howarth, J., Litchfield, N., Cochran, U., Turnbull, J., Dowling, L., et al. (2019). Geological evidence for past large earthquakes and tsunamis along the Hikurangi subduction margin, New Zealand. *Marine Geology*, *412*, 139–172. https://doi.org/10.1016/j.margeo.2019.03.004

Coffin, M. F., & Eldholm, O. (1994). Large igneous provinces: Crustal structure, dimensions, and external consequences. *Reviews of Geophysics*, *32*(1), 1–36. https://doi.org/10.1029/93rg02508

Collot, J. Y., Delteil, J., Lewis, K. B., Davy, B., Lamarche, G., Audru, J. C., et al. (1996). From oblique subduction to intra-continental transpression: Structures of the southern Kermadec-Hikurangi margin from multibeam bathymetry, side-scan sonar and seismic reflection. *Marine Geophysical Researches*, *18*(2/4), 357–381. https://doi.org/10.1007/bf00286085

Collot, J. Y., Lewis, K., Lamarche, G., & Lallemand, S. (2001). The giant Ruatoria debris avalanche on the northern Hikurangi margin, New Zealand: Result of oblique seamount subduction. *Journal of Geophysical Research: Solid Earth*, *106*(B9), 19271–19297. https://doi.org/10.1029/2001jb900004

Crawford, A. J., Meffre, S., & Symonds, P. (2003). 120 to 0 Ma tectonic evolution of the southwest Pacific and analogous geological evolution of the 600 to 220 Ma Tasman fold belt system. *Geological Society of Australia Special Publication*, *22*, 377–397.

Davy, B., Hoernle, K., & Werner, R. (2008). Hikurangi Plateau: Crustal structure, rifted formation, and Gondwana subduction history. *Geochemistry, Geophysics, Geosystems*, *9*(7), Q07004. https://doi.org/10.01029/02007GC001855

Delano, J., Howell, A., Clark, K., & Stahl, T. (2023). Upper plate faults may contribute to the paleoseismic subsidence record along the central Hikurangi subduction zone, Aotearoa New Zealand. *Geochemistry, Geophysics, Geosystems*, *24*(10), e2023GC011060. https://doi.org/10.1029/2023gc011060

DeMets, C., Gordon, R. G., & Argus, D. F. (2010). Geologically current plate motions. *Geophysical Journal International*, *181*(1), 1–80. https://doi.org/10.1111/j.1365-246x.2009.04491.x

Dimitrova, L., Wallace, L., Haines, A., & Williams, C. (2016). High-resolution view of active tectonic deformation along the Hikurangi subduction margin and the Taupo Volcanic Zone, New Zealand. *New Zealand Journal of Geology and Geophysics*, *59*(1), 43–57. https://doi.org/10.1080/00288306.2015.1127823

Doser, D. I., & Webb, T. H. (2003). Source parameters of large historical (1917–1961) earthquakes, North Island, New Zealand. *Geophysical Journal International*, *152*(3), 795–832. https://doi.org/10.1046/j.1365-246x.2003.01895.x

Downes, G. (2006). The 1904 Ms6. 8 Mw7. 0-7.2 Cape Turnagain, New Zealand, earthquake. *Bulletin of the New Zealand Society for Earthquake Engineering*, *39*(4), 183–207. https://doi.org/10.5459/bnzsee.39.4.183-207

Downes, G., Webb, T. H., Chauge-Godd, C., Darby, D., & Barnett, A. (2000). *The March 25 and may 17 1947 Gisborne earthquakes and tsunami: Implications for tsunami hazard for east coast, North Island, New Zealand*. Joint IOC/IUGG International Workshop: Tsunami Risk Assessment and Beyond 2000 - Theory, Practice and Plans.

Eberhart-Phillips, D., & Bannister, S. (2015). 3-D imaging of the northern Hikurangi subduction zone, New Zealand: Variations in subducted sediment, slab fluids and slow slip. *Geophysical Journal International*, *201*(2), 838–855. https://doi.org/10.1093/gji/ggv057

Eberhart-Phillips, D., Bannister, S., & Reyners, M. (2017). Deciphering the 3-D distribution of fluid along the shallow Hikurangi subduction zone using P-and S-wave attenuation. *Geophysical Journal International*, *211*(2), 1032–1045. https://doi.org/10.1093/gji/ggx348

Eberhart-Phillips, D., Bannister, S., Reyners, M., & Bourguignon, S. (2022). New Zealand Wide model 2.3 seismic velocity model for New Zealand (vlnzwide2.3). *Zenodo*, *10*

Fagereng, A., & Ellis, S. (2009). On factors controlling the depth of interseismic coupling on the Hikurangi subduction interface, New Zealand. *Earth and Planetary Science Letters*, *278*(1–2), 120–130. https://doi.org/10.1016/j.epsl.2008.11.033

Gase, A. C., Bangs, N., Van Avendonk, H. J., Bassett, D., Henrys, S., Barker, D., et al. (2021). Crustal structure of the northern Hikurangi margin, New Zealand: Variable accretion and upper plate strength influenced by rough subduction. *Journal of Geophysical Research B: Solid Earth*.

Gase, A. C., Bangs, N. L., Saffer, D. M., Han, S., Miller, P. K., Bell, R. E., et al. (2023). Subducting volcaniclastic-rich upper crust supplies fluids for shallow megathrust and slow slip. *Science Advances*, *9*(33), eadh0150. https://doi.org/10.1126/sciadv.adh0150

Gase, A. C., Bangs, N. L., Van Avendonk, H. J., Bassett, D., Henrys, S., Arai, R., et al. (2024). Volcanic crustal structure of the western Hikurangi Plateau (New Zealand) from marine seismic reflection imaging. *Geosphere*, *20*(3), 935–964. https://doi.org/10.1130/ges02744.1

Gase, A. C., Bangs, N. L., Van Avendonk, H. J., Bassett, D., & Henrys, S. A. (2022). Hikurangi megathrust slip behavior influenced by lateral variability in sediment subduction. *Geology*, *50*(10), 1145–1149. https://doi.org/10.1130/g50261.1

Gase, A. C., Van Avendonk, H. J., Bangs, N. L., Luckie, T. W., Barker, D. H., Henrys, S. A., et al. (2019). Seismic evidence of magmatic rifting in the offshore Taupo Volcanic Zone, New Zealand. *Geophysical Research Letters*, *46*(22), 12949–12957. https://doi.org/10.1029/2019gl085269

Ghisetti, F., Barnes, P., Ellis, S., Plaza-Faverola, A., & Barker, D. H. N. (2016). The last 2 Myr of accretionary wedge construction in the central Hikurangi margin (North Island, New Zealand): Insights from structural modeling. *Geochemistry, Geophysics, Geosystems*, *17*(7), 2661–2686. https://doi.org/10.1002/2016gc006341

Gns Science (2024). GeoNet Aotearoa New Zealand seismic digital waveform dataset [Dataset]. *GNS Science, GeoNet*. https://doi.org/10.21420/G19Y-9D40

GNS Science. (2017). Seismogenesis at Hikurangi integrated research experiment (SHIRE) offshre data. *GNS Science Dataset Catalogue*. [Dataset]. https://doi.org/10.21420/TQ67-8F60

Haines, A. J., & Wallace, L. M. (2020). New Zealand-Wide geodetic strain rates using a physics-based approach. *Geophysical Research Letters*, *47*(1), e2019GL084606. https://doi.org/10.1029/2019gl084606

Heise, W., Bertrand, E. A., Caldwell, T. G., Ogawa, Y., Bannister, S., Bennie, S. L., et al. (2023). An electrical resistivity image of the Hikurangi subduction margin. *Geophysical Journal International*, *235*(2), 1552–1564. https://doi.org/10.1093/gji/ggad313

Heise, W., Caldwell, T. G., Bannister, S., Bertrand, E., Ogawa, Y., Bennie, S., & Ichihara, H. (2017). Mapping subduction interface coupling using magnetotellurics: Hikurangi margin, New Zealand. *Geophysical Research Letters*, *44*(18), 9261–9266. https://doi.org/10.1002/2017gl074641

Henrys, S. (2003). *New Zealand North Island GeopHysical transect (NIGHT): Field acquisition report*. Institute of Geological and Nuclear Sciences.

Henrys, S., Eberhart-Phillips, D., Bassett, D., Sutherland, R., Okaya, D., Savage, M., et al. (2020). Upper Plate heterogeneity along the southern Hikurangi margin, New Zealand. *Geophysical Research Letters*, *47*(4), e2019GL085511. https://doi.org/10.1029/2019gl085511

Henrys, S., Wech, A., Sutherland, R., Stern, T., Savage, M., Sato, H., et al. (2013). SAHKE geophysical transect reveals crustal and subduction zone structure at the southern Hikurangi margin, New Zealand. *Geochemistry, Geophysics, Geosystems*, *14*(7), 2063–2083. https://doi.org/10.1002/ggge.20136

Herath, P., Stern, T. A., Savage, M. K., Bassett, D., Henrys, S., & Boulton, C. (2020). Hydration of the crust and upper mantle of the Hikurangi Plateau as it subducts at the southern Hikurangi margin. *Earth and Planetary Science Letters*, *541*, 116271. https://doi.org/10.1016/j.epsl.2020.116271

Heron, D. (2014). Geological map of New Zealand: Institute of geological and nuclear sciences 1: 250,000 geological map 1: Lower hutt: New Zealand, GNS science, scale, *1*(250000), 1.

Heron, D. W., Edbrooke, S., Forsyth, P., & Jongens, R. (2015). Geological map of New Zealand, 1: 1 000 000, institute of geological and nuclear sciences limited.

Herzer, R. H., Barker, D., Roest, W., & Mortimer, N. (2011). Oligocene-Miocene spreading history of the northern South Fiji Basin and implications for the evolution of the New Zealand plate boundary. *Geochemistry, Geophysics, Geosystems*, *12*(2). https://doi.org/10.1029/2010gc003291

Hetland, E., & Simons, M. (2010). Post-seismic and interseismic fault creep II: Transient creep and interseismic stress shadows on megathrusts. *Geophysical Journal International*, *181*(1), 99–112. https://doi.org/10.1111/j.1365-246x.2009.04482.x

Hirschberg, H., & Sutherland, R. (2022). A kinematic model of Quaternary fault slip rates and distributed deformation at the New Zealand plate boundary. *Journal of Geophysical Research: Solid Earth*, *127*(11), e2022JB024828. https://doi.org/10.1029/2022jb024828

Hoernle, K., Hauff, F., Van den Bogaard, P., Werner, R., Mortimer, N., Geldmacher, J., et al. (2010). Age and geochemistry of volcanic rocks from the Hikurangi and Manihiki oceanic Plateaus. *Geochimica et Cosmochimica Acta*, *74*(24), 7196–7219. https://doi.org/10.1016/j.gca.2010.09.030

Hu, Y., & Wang, K. (2008). Coseismic strengthening of the shallow portion of the subduction fault and its effects on wedge taper. *Journal of Geophysical Research*, *113*(B12). https://doi.org/10.1029/2008jb005724

Hyndman, R., & Wang, K. (1995). The rupture zone of Cascadia great earthquakes from current deformation and the thermal regime. *Journal of Geophysical Research: Solid Earth*, *100*(B11), 22133–22154. https://doi.org/10.1029/95jb01970

Jiao, R., Herman, F., & Seward, D. (2017). Late Cenozoic exhumation model of New Zealand: Impacts from tectonics and climate. *Earth-Science Reviews*, *166*, 286–298. https://doi.org/10.1016/j.earscirev.2017.01.003

Kamei, R., Pratt, R. G., & Tsuji, T. (2012). Waveform tomography imaging of a megasplay fault system in the seismogenic Nankai subduction zone. *Earth and Planetary Science Letters*, *317*, 343–353. https://doi.org/10.1016/j.epsl.2011.10.042

Kanamori, H. (1981). The nature of seismicity patterns before large earthquakes: Earthquake Prediction (pp. 1–19).

Kaneko, Y., Avouac, J.-P., & Lapusta, N. (2010). Towards inferring earthquake patterns from geodetic observations of interseismic coupling. *Nature Geoscience*, *3*(5), 363–369. https://doi.org/10.1038/ngeo843

Kaneko, Y., & Chow, B. (2017). Broadband East coast network (BEACON). *International federation of digital seismograph networks*.

Kaneko, Y., Ito, Y., Chow, B., Wallace, L. M., Tape, C., Grapenthin, R., et al. (2019). Ultra-long duration of seismic ground motion arising from a thick, low-velocity sedimentary wedge. *Journal of Geophysical Research: Solid Earth*, *124*(10), 10347–10359. https://doi.org/10.1029/2019jb017795

Kelleher, J., & McCann, W. (1976). Buoyant zones, great earthquakes, and unstable boundaries of subduction. *Journal of Geophysical Research*, *81*(26), 4885–4896. https://doi.org/10.1029/jb081i026p04885

Kopp, H., & Kukowski, N. (2003). Backstop geometry and accretionary mechanics of the Sunda margin. *Tectonics*, *22*(6). https://doi.org/10.1029/2002tc001420

Langridge, R., Ries, W., Litchfield, N., Villamor, P., Van Dissen, R., Barrell, D., et al. (2016). The New Zealand active faults database. *New Zealand Journal of Geology and Geophysics*, *59*(1), 86–96. https://doi.org/10.1080/00288306.2015.1112818

Lay, T., Kanamori, H., Ammon, C. J., Koper, K. D., Hutko, A. R., Ye, L., et al. (2012). Depth-varying rupture properties of subduction zone megathrust faults. *Journal of Geophysical Research*, *117*(B4). https://doi.org/10.1029/2011jb009133

Lewis, K. B., Collot, J. Y., & Lallemand, S. E. (1998). The dammed Hikurangi trough: A channel-fed trench blocked by subducting seamounts and their wake avalanches (New Zealand-France GeodyNZ Project). *Basin Research*, *10*(4), 441–468. https://doi.org/10.1046/j.1365-2117.1998.00080.x

Lewis, K. B., Lallemand, S. E., & Carter, L. (2004). Collapse in a quaternary shelf basin off East Cape, New Zealand: Evidence for passage of a subducted seamount inboard of the Ruatoria giant avalanche. *New Zealand Journal of Geology and Geophysics*, *47*(3), 415–429. https://doi.org/10.1080/00288306.2004.9515067

Litchfield, N., Ellis, S., Berryman, K., & Nicol, A. (2007). Insights into subduction-related uplift along the Hikurangi Margin, New Zealand, using numerical modeling. *Journal Of Geophysical Research-Earth Surface*, *112*(F2). https://doi.org/10.1029/2006JF000535

Litchfield, N., Van Dissen, R., Sutherland, R., Barnes, P., Cox, S., Norris, R., et al. (2014). A model of active faulting in New Zealand. *New Zealand Journal of Geology and Geophysics*, *57*(1), 32–56. https://doi.org/10.1080/00288306.2013.854256

Little, T. A., & Roberts, A. P. (1997). Distribution and mechanism of Neogene to present-day vertical axis rotations, Pacific-Australian plate boundary zone, South Island, New Zealand. *Journal of Geophysical Research*, *102*(B9), 20447–20468. https://doi.org/10.1029/97jb01279

Liu, X., & Zhao, D. (2018). Upper and lower plate controls on the great 2011 Tohoku-oki earthquake. *Science Advances*, *4*(6), eaat4396. https://doi.org/10.1126/sciadv.aat4396

McArthur, A. D., Claussmann, B., Bailleul, J., Clare, A., & McCaffrey, W. (2020). Variation in syn-subduction sedimentation patterns from inner to outer portions of deep-water fold and thrust belts: Examples from the Hikurangi subduction margin of New Zealand. *Geological Society, London, Special Publications*, *490*(1), 285–310. https://doi.org/10.1144/sp490-2018-95

Meffre, S., Falloon, T. J., Crawford, T. J., Hoernle, K., Hauff, F., Duncan, R. A., et al. (2012). Basalts erupted along the Tongan fore arc during subduction initiation: Evidence from geochronology of dredged rocks from the Tonga fore arc and trench. *Geochemistry, Geophysics, Geosystems*, *13*(12). https://doi.org/10.1029/2012gc004335

Mitchell, J., Mackay, K., Neil, H., Mackay, E., Pallentin, A., & Notman, P. (2012). Undersea New Zealand, 1: 5,000,000: NIWA chart, miscellaneous series, v. 92.

Miura, S., Takahashi, N., Nakanishi, A., Tsuru, T., Kodaira, S., & Kaneda, Y. (2005). Structural characteristics off Miyagi forearc region, the Japan Trench seismogenic zone, deduced from a wide-angle reflection and refraction study. *Tectonophysics*, *407*(3), 165–188. https://doi.org/10.1016/j.tecto.2005.08.001

Mochizuki, K., Sutherland, R., Henrys, S., Bassett, D., Van Avendonk, H., Arai, R., et al. (2019). Recycling of depleted continental mantle by subduction and plumes at the Hikurangi Plateau large igneous province, southwestern Pacific Ocean. *Geology*, *47*(8), 795–798. https://doi.org/10.1130/g46250.1

Moore, P., & Speden, I. (1979). Stratigraphy, structure, and inferred environments of deposition of the Early Cretaceous sequence, eastern Wairarapa, New Zealand. *New Zealand Journal of Geology and Geophysics*, *22*(4), 417–433. https://doi.org/10.1080/00288306.1979.10424150

Moore, P. R., & Speden, I. G. (1984). The early cretaceous (Albian) sequence of eastern Wairarapa, New Zealand.

Mortimer, N. (2004). New Zealand's geological foundations. *Gondwana Research*, *7*(1), 261–272. https://doi.org/10.1016/s1342-937x(05)70324-5

Mortimer, N., Herzer, R. H., Gans, P. B., Laporte-Magoni, C., Calvert, A. T., & Bosch, D. (2007). Oligocene–miocene tectonic evolution of the South Fiji Basin and Northland plateau, SW Pacific ocean: Evidence from petrology and dating of dredged rocks. *Marine Geology*, *237*(1–2), 1–24. https://doi.org/10.1016/j.margeo.2006.10.033

Mortimer, N., & Parkinson, D. (1996). Hikurangi Plateau; a cretaceous large igneous province in the southwest Pacific ocean. *Journal of Geophysical Research - B: Solid Earth and Planets*, *101*(B1), 687–696. https://doi.org/10.1029/95jb03037

Moser, T. (1991). Shortest path calculation of seismic rays. *Geophysics*, *56*(1), 59–67. https://doi.org/10.1190/1.1442958

Mountjoy, J. J., & Barnes, P. M. (2011). Active upper plate thrust faulting in regions of low plate interface coupling, repeated slow slip events, and coastal uplift: Example from the Hikurangi Margin, New Zealand. *Geochemistry, Geophysics, Geosystems*, *12*(1). https://doi.org/10.1029/2010gc003326

Nakanishi, A., Kodaira, S., Park, J.-O., & Kaneda, Y. (2002). Deformable backstop as seaward end of coseismic slip in the Nankai Trough seismogenic zone. *Earth and Planetary Science Letters*, *203*(1), 255–263. https://doi.org/10.1016/s0012-821x(02)00866-x

Nicol, A., Mazengarb, C., Chanier, F., Rait, G., Uruski, C. I., & Wallace, L. M. (2007). Tectonic evolution of the active Hikurangi subduction margin, New Zealand, since the Oligocene. *Tectonics*, *26*(4), TC4002. https://doi.org/10.1029/2006TC002090

Nishimura, T., Yokota, Y., Tadokoro, K., & Ochi, T. (2018). Strain partitioning and interplate coupling along the northern margin of the Philippine sea plate, estimated from global navigation satellite system and global positioning system-acoustic data. *Geosphere*, *14*(2), 535–551. https://doi.org/10.1130/ges01529.1

Oleskevich, D., Hyndman, R., & Wang, K. (1999). The updip and downdip limits to great subduction earthquakes: Thermal and structural models of Cascadia, south Alaska, SW Japan, and Chile. *Journal of Geophysical Research: Solid Earth*, *104*(B7), 14965–14991. https://doi.org/10.1029/1999jb900060

Orr, D., Sutherland, R., & Stratford, W. (2020). Eocene to Miocene subduction initiation recorded in stratigraphy of Reinga Basin, northwest New Zealand. *Tectonics*, *39*(2), e2019TC005899. https://doi.org/10.1029/2019tc005899

Pedley, K. L., Barnes, P. M., Pettinga, J. R., & Lewis, K. B. (2010). Seafloor structural geomorphic evolution of the accretionary frontal wedge in response to seamount subduction, Poverty Indentation, New Zealand. *Marine Geology*, *270*(1–4), 119–138. https://doi.org/10.1016/j.margeo.2009.11.006

Pizer, C., Clark, K., Howarth, J., Garrett, E., Wang, X., Rhoades, D., & Woodroffe, S. (2021). Paleotsunamis on the southern Hikurangi subduction zone, New Zealand, show regular recurrence of large subduction earthquakes: The Seismic Record. *The Seismic Record*, *1*(2), 75–84. https://doi.org/10.1785/0320210012

Pizer, C., Clark, K., Howarth, J., Howell, A., Delano, J., Hayward, B. W., & Litchfield, N. (2023). *A 5000 yr record of coastal uplift and subsidence reveals multiple source faults for past earthquakes on the central Hikurangi margin*. Geological Society of America Bulletin.

Plaza-Faverola, A., Henrys, S., Pecher, I., Wallace, L., & Klaeschen, D. (2016). Splay fault branching from the Hikurangi subduction shear zone: Implications for slow slip and fluid flow. *Geochemistry, Geophysics, Geosystems*, *17*(12), 5009–5023. https://doi.org/10.1002/2016gc006563

Pondard, N., & Barnes, P. M. (2010). Structure and paleoearthquake records of active submarine faults, Cook Strait, New Zealand: Implications for fault interactions, stress loading, and seismic hazard. *Journal of Geophysical Research*, *115*(B12). https://doi.org/10.1029/2010jb007781

Price, R. C., Gamble, J. A., Smith, I. E., Stewart, R. B., Eggins, S., & Wright, I. C. (2005). An integrated model for the temporal evolution of andesites and rhyolites and crustal development in New Zealand's North Island. *Journal of Volcanology and Geothermal Research*, *140*(1–3), 1–24. https://doi.org/10.1016/j.jvolgeores.2004.07.013

Reyners, M., & Eberhart-Phillips, D. (2009). Small earthquakes provide insight into plate coupling and fluid distribution in the Hikurangi subduction zone, New Zealand. *Earth and Planetary Science Letters*, *282*(1), 299–305. https://doi.org/10.1016/j.epsl.2009.03.034

Reyners, M., Eberhart-Phillips, D., & Bannister, S. (2011). Tracking repeated subduction of the Hikurangi Plateau beneath New Zealand. *Earth and Planetary Science Letters*, *311*(1), 165–171. https://doi.org/10.1016/j.epsl.2011.09.011

Robinson, D. P., Das, S., & Watts, A. B. (2006). Earthquake rupture stalled by a subducting fracture zone. *Science*, *312*(5777), 1203–1205. https://doi.org/10.1126/science.1125771

Rowan, C. J., & Roberts, A. P. (2008). Widespread remagnetizations and a new view of Neogene tectonic rotations within the Australia-Pacific plate boundary zone, New Zealand. *Journal of Geophysical Research: Solid Earth*, *113*(B3). https://doi.org/10.1029/2006JB004594

Sallarès, V., Prada, M., Riquelme, S., Meléndez, A., Calahorrano, A., Grevemeyer, I., & Ranero, C. R. (2021). Large slip, long duration, and moderate shaking of the Nicaragua 1992 tsunami earthquake caused by low near-trench rock rigidity. *Science Advances*, *7*(32), eabg8659. https://doi.org/10.1126/sciadv.abg8659

Sallarès, V., & Ranero, C. R. (2019). Upper-plate rigidity determines depth-varying rupture behaviour of megathrust earthquakes. *Nature*, *576*(7785), 96–101. https://doi.org/10.1038/s41586-019-1784-0

Scherwath, M., Kopp, H., Flueh, E. R., Henrys, S. A., Sutherland, R., Stagpoole, V. M., et al. (2010). Fore-arc deformation and underplating at the northern Hikurangi margin, New Zealand. *Journal of Geophysical Research B: Solid Earth*, *115*(6). https://doi.org/10.1029/2009jb006645

Seebeck, H., Strogen, D. P., Nicol, A., Hines, B. R., & Bland, K. J. (2023). A tectonic reconstruction model for Aotearoa-New Zealand from the mid-Late Cretaceous to the present day. *New Zealand Journal of Geology and Geophysics*, *67*(4), 1–24. https://doi.org/10.1080/00288306.2023.2239175

Seebeck, H., Van Dissen, R., Litchfield, N., Barnes, P. M., Nicol, A., Langridge, R., et al. (2024). The New Zealand Community Fault Model–version 1.0: An improved geological foundation for seismic hazard modelling. *New Zealand Journal of Geology and Geophysics*, *67*(2), 209–229. https://doi.org/10.1080/00288306.2023.2181362

Shreedharan, S., Saffer, D., Wallace, L. M., & Williams, C. (2023). Ultralow frictional healing explains recurring slow slip events. *Science*, *379*(6633), 712–717. https://doi.org/10.1126/science.adf4930

Skarbek, R. M., Rempel, A. W., & Schmidt, D. A. (2012). Geologic heterogeneity can produce aseismic slip transients. *Geophysical Research Letters*, *39*(21). https://doi.org/10.1029/2012gl053762

Stern, T., Lamb, S., Moore, J. D., Okaya, D., & Hochmuth, K. (2020). High mantle seismic P-wave speeds as a signature for gravitational spreading of superplumes. *Science Advances*, *6*(22), eaba7118. https://doi.org/10.1126/sciadv.aba7118

Stevens, D. E., McNeill, Y., Henstock, T., Barnes, P. M., Crutchley, G., Bangs, N., et al. (2024). Structural variation along the southern Hikurangi subduction zone, Aotearoa New Zealand, from seismic reflection and retro-deformation analysis. *Tectonics*, *43*(7), e2023TC008212. https://doi.org/10.1029/2023tc008212

Stratford, W., & Stern, T. (2006). Crust and upper mantle structure of a continental backarc: Central North Island, New Zealand. *Geophysical Journal International*, *166*(1), 469–484. https://doi.org/10.1111/j.1365-246x.2006.02967.x

Sun, T., Saffer, D., & Ellis, S. (2020). Mechanical and hydrological effects of seamount subduction on megathrust stress and slip. *Nature Geoscience*, *13*(3), 249–255. https://doi.org/10.1038/s41561-020-0542-0

Sun, T., Wang, K., Iinuma, T., Hino, R., He, J., Fujimoto, H., et al. (2014). Prevalence of viscoelastic relaxation after the 2011 Tohoku-oki earthquake. *Nature*, *514*(7520), 84–87. https://doi.org/10.1038/nature13778

Sutherland, R., Dickens, G. R., Blum, P., Agnini, C., Alegret, L., Asatryan, G., et al. (2020). Continental-scale geographic change across Zealandia during Paleogene subduction initiation: Geology. *Geology*, *48*(5), 419–424. https://doi.org/10.1130/g47008.1

Sutherland, R., Stagpoole, V., Uruski, C., Kennedy, C., Bassett, D., Henrys, S., et al. (2009). Reactivation of tectonics, crustal underplating, and uplift after 60 Myr of passive subsidence, Raukumara Basin, Hikurangi-Kermadec fore arc, New Zealand: Implications for global growth and recycling of continents. *Tectonics*, *28*(5). https://doi.org/10.1029/2008tc002356

Thornley, S. (1996). Neogene tectonics of Raukumara Peninsula, northern Hikurangi margin.

Timm, C., Hoernle, K., Werner, R., Hauff, F., van den Bogaard, P., White, J., et al. (2010). Temporal and geochemical evolution of the Cenozoic intraplate volcanism of Zealandia. *Earth-Science Reviews*, *98*(1–2), 38–64. https://doi.org/10.1016/j.earscirev.2009.10.002

Tinti, E., Bizzarri, A., & Cocco, M. (2005). Modeling the dynamic rupture propagation on heterogeneous faults with rate-and state-dependent friction. *Annals of Geophysics*.

Tozer, B., Stern, T., Lamb, S., & Henrys, S. (2017). Crust and upper-mantle structure of Wanganui Basin and southern Hikurangi margin, North Island, New Zealand as revealed by active source seismic data. *Geophysical Journal International*, *211*(2), 718–740. https://doi.org/10.1093/gji/ggx303

Ulrich, T., Gabriel, A.-A., & Madden, E. H. (2022). Stress, rigidity and sediment strength control megathrust earthquake and tsunami dynamics. *Nature Geoscience*, *15*(1), 67–73. https://doi.org/10.1038/s41561-021-00863-5

van Avendonk, H., Gase, A., & Bangs, N. (2023). Structural variations and seismogenic character of the Hikurangi margin, New Zealand. In *Seismological society of America annual meeting: San juan Puerto Rico*.

Van Avendonk, H. J., Harding, A. J., Orcutt, J. A., & Holbrook, W. S. (2001). Hybrid shortest path and ray bending method for traveltime and raypath calculations. *Geophysics*, *66*(2), 648–653. https://doi.org/10.1190/1.1444955

Van Avendonk, H. J., Shillington, D. J., Holbrook, W. S., & Hornbach, M. J. (2004). Inferring crustal structure in the Aleutian island arc from a sparse wide-angle seismic data set. *Geochemistry, Geophysics, Geosystems*, *5*(8). https://doi.org/10.1029/2003gc000664

van de Lagemaat, S. H., Mering, J. A., & Kamp, P. J. (2022). Geochemistry of syntectonic carbonate veins within Late Cretaceous turbidites, Hikurangi Margin (New Zealand): Implications for a mid-Oligocene age of subduction initiation. *Geochemistry, Geophysics, Geosystems*, *23*(5), e2021GC010125. https://doi.org/10.1029/2021gc010125

Walcott, R. (1989). *Paleomagnetically observed rotations along the Hikurangi margin of New Zealand, Paleomagnetic rotations and continental deformation* (pp. 459–471). Springer.

Walcott, R. I. (1978). Present tectonics and late Cenozoic evolution of New Zealand. *Geophysical Journal of the Royal Astronomical Society*, *52*(1), 137–164. https://doi.org/10.1111/j.1365-246x.1978.tb04225.x

Walcott, R. I., Mumme, T. C., & Christoffel, D. A. (1981). Bending within the axial tectonic belt of New Zealand in the last 9 Myr from paleomagnetic data. *Earth and Planetary Science Letters*, *52*(2), 427–434. https://doi.org/10.1016/0012-821x(81)90195-3

Wallace, L., Barnes, P., Beavan, J., Van Dissen, R., Litchfield, N., Mountjoy, J., et al. (2012). The kinematics of a transition from subduction to strike-slip: An example from the central New Zealand plate boundary. *Journal of Geophysical Research*, *117*(B2). https://doi.org/10.1029/2011jb008640

Wallace, L. M. (2020). Slow slip events in New Zealand. *Annual Review of Earth and Planetary Sciences*, *48*(1), 175–203. https://doi.org/10.1146/annurev-earth-071719-055104

Wallace, L. M., & Beavan, J. (2010). Diverse slow slip behavior at the Hikurangi subduction margin, New Zealand. *Journal of Geophysical Research*, *115*(B12). https://doi.org/10.1029/2010jb007717

Wallace, L. M., Beavan, J., Bannister, S., & Williams, C. (2012). Simultaneous long-term and short-term slow slip events at the Hikurangi subduction margin, New Zealand: Implications for processes that control slow slip event occurrence, duration, and migration. *Journal of Geophysical Research*, *117*, B11. https://doi.org/10.1029/2012jb009489

Wallace, L. M., Beavan, J., McCaffrey, R., & Darby, D. (2004). Subduction zone coupling and tectonic block rotations in the North Island, New Zealand. *Journal of Geophysical Research*, *109*(B12). https://doi.org/10.1029/2004JB003241

Wallace, L. M., & Eberhart-Phillips, D. (2013). Newly observed, deep slow slip events at the central Hikurangi margin, New Zealand: Implications for downdip variability of slow slip and tremor, and relationship to seismic structure. *Geophysical Research Letters*, *40*(20), 5393–5398. https://doi.org/10.1002/2013gl057682

Wallace, L. M., Fagereng, Å., & Ellis, S. (2012). Upper plate tectonic stress state may influence interseismic coupling on subduction megathrusts: Geology. *Geology*, *40*(10), 895–898. https://doi.org/10.1130/g33373.1

Wallace, L. M., Hreinsdottir, S., Ellis, S., Hamling, I., D'Anastasio, E., & Denys, P. (2018). Triggered slow slip and afterslip on the southern Hikurangi subduction zone following the Kaikōura earthquake. *Geophysical Research Letters*, *45*(10), 4710–4718. https://doi.org/10.1002/2018gl077385

Wallace, L. M., Webb, S. C., Ito, Y., Mochizuki, K., Hino, R., Henrys, S., et al. (2016). Slow slip near the trench at the Hikurangi subduction zone, New Zealand. *Science*, *352*(6286), 701–704. https://doi.org/10.1126/science.aaf2349

Wang, K., & Bilek, S. L. (2011). Do subducting seamounts generate or stop large earthquakes? *Geology*, *39*(9), 819–822. https://doi.org/10.1130/g31856.1

Webb, T. H., & Anderson, H. (1998). Focal mechanisms of large earthquakes in the north Island of New Zealand: Slip partitioning at an oblique active margin. *Geophysical Journal International*, *134*(1), 40–86. https://doi.org/10.1046/j.1365-246x.1998.00531.x

Wessel, P., Luis, J., Uieda, L., Scharroo, R., Wobbe, F., Smith, W., & Tian, D. (2019). The generic mapping tools version 6. *Geochemistry, Geophysics, Geosystems*, *20*(11), 5556–5564. https://doi.org/10.1029/2019gc008515

Wessel, P., & Smith, W. H. (1991). Free software helps map and display data. *Eos, Transactions American Geophysical Union*, *72*(41), 441–446. https://doi.org/10.1029/90eo00319

Williams, C. A., Eberhart-Phillips, D., Bannister, S., Barker, D. H., Henrys, S., Reyners, M., & Sutherland, R. (2013). Revised interface geometry for the Hikurangi subduction zone, New Zealand. *Seismological Research Letters*, *84*(6), 1066–1073. https://doi.org/10.1785/0220130035

Williams, C. A., & Wallace, L. M. (2018). The impact of realistic elastic properties on inversions of shallow subduction interface slow slip events using seafloor geodetic data. *Geophysical Research Letters*, *45*(15), 7462–7470. https://doi.org/10.1029/2018gl078042

Wilson, C., Houghton, B., McWilliams, M., Lanphere, M. A., Weaver, S., & Briggs, R. (1995). Volcanic and structural evolution of Taupo volcanic zone, New Zealand: A review. *Journal of Volcanology and Geothermal Research*, *68*(1–3), 1–28. https://doi.org/10.1016/0377-0273(95)00006-g